European Journal of Medicinal Chemistry 264 (2024) 116021

Contents lists available at ScienceDirect

European Journal of Medicinal Chemistry

journal homepage: www.elsevier.com/locate/ejmech

Research paper

Biological evaluation of carbohydrate-based aprepitant analogs for neuroblastoma treatment

Victoria Valdivia [a], Rocío Recio [a,*], Patricia Lerena [a], Esther Pozo [a], Rosario Serrano [b], Raúl Calero [b], Cristina Pintado [b], Manuel Pernia Leal [a], Nazaret Moreno-Rodríguez [a], Juan Ángel Organero [c], Noureddine Khiar [d], Inmaculada Fernández [a,**]

[a] Departamento de Química Orgánica y Farmacéutica, Facultad de Farmacia, Universidad de Sevilla, C/ Profesor García González, 2, 41012, Sevilla, Spain
[b] Departamento de Química Inorgánica, Química Orgánica y Bioquímica, Facultad de Ciencias Ambientales y Bioquímica, Universidad de Castilla-La Mancha, Toledo, Spain
[c] Departamento de Química Física, Facultad de Ciencias Ambientales y Bioquímicas and INAMOL, Universidad de Castilla-La Mancha, Avda. Carlos III, s.n., 45071, Toledo, Spain
[d] Instituto de Investigaciones Químicas (IIQ), CSIC-Universidad de Sevilla. Avda. Américo Vespucio, 49, Isla de la Cartuja, 41092, Sevilla, Spain

ARTICLE INFO

Keywords:
Neuroblastoma
Aprepitant
NK1R antagonists
Carbohydrate-based derivatives

ABSTRACT

Different studies using Aprepitant, a NK1R antagonist currently used as a clinical drug for treating chemotherapy-related nausea and vomiting, have demonstrated that pharmacological inhibition of NK1R effectively reduces the growth of several tumor types such as neuroblastoma (NB). In a previous work, we demonstrated that a series of carbohydrate-based Aprepitant analogs, derived from either D-galactose or L-arabinose, have shown high affinity and NK1R antagonistic activity with a broad-spectrum anticancer activity and an important selectivity. In this new study, we explore the selective cytotoxic effects of these derivatives for the treatment of NB. Furthermore, we describe the design and stereoselective synthesis of a new generation of D-glucose derivatives as Aprepitant analogs, supported by docking studies. This approach showed that most of our carbohydrate-based analogs are significantly more selective than Aprepitant. The galactosyl derivative **2α**, has demonstrated a marked *in vitro* selective cytotoxic activity against NB, with IC_{50} values in the same range as those of Aprepitant and its prodrug Fosaprepitant. Interestingly, the derivative **2α** has shown similar apoptotic effect to that of Aprepitant.

Moreover, we can select the glucosyl amino derivative **10α** as an interesting hit exhibiting higher *in vitro* cytotoxic activity against NB than Aprepitant, being 1.2 times more selective.

1. Introduction

Neuroblastoma (NB) is the most common extracranial solid tumor in children. It is the most frequent malignancy during infancy, accounting for >20% of cancers diagnosed during the first year of life and causing up to 10% of childhood cancer mortality [1]. A hallmark of neuroblastoma is its heterogeneity showing a high variability in its clinical presentation, course, and prognosis. It ranges from patients with tumors that can spontaneously regress, children with localized tumors and good overall survival with limited chemotherapy, to patients with widely disseminated disease and bad outcome despite intensive multimodal chemoradiotherapy [2]. While remarkable improvements have been made for children with lower-stage disease, children with high-risk neuroblastoma have less than 40% of survival. The biological and clinical heterogeneity of these tumors demands novel biomarkers and therapeutic targets to achieve an effective treatment for high-risk patients.

Recently, neurokinin 1 receptor (NK1R) has become an interesting target in a large variety of childhood cancers such as NB [3–5]. The neurokinins are one of the largest conserved families of peptides involved in neurotransmission and inflammatory processes. There are three different types of neurokinin receptors: NK1R, NK2R and NK3R. NK1R activation by substance P (SP) is linked among other physiological and biological processes to cell growth and differentiation and has been

* Corresponding author.
** Corresponding author.
E-mail address: rrecioj@us.es (R. Recio).

https://doi.org/10.1016/j.ejmech.2023.116021
Received 31 October 2023; Received in revised form 24 November 2023; Accepted 29 November 2023
Available online 5 December 2023

proposed to be involved in oncogenesis and tumoral angiogenesis [6]. Furthermore, NK1R presents two splice variants: a full-length variant (fl-NK1R) and a truncated variant (tr-NK1R) [5]. The association between the expression of each splice variant and the overall prognosis of NB has been analyzed. These studies revealed that there was no statistically significant difference for either splice variant. *In vitro* and *in vivo* studies using NK1R antagonists such as Aprepitant, currently used as a clinical drug for the treatment of chemotherapy-related nausea and vomiting, demonstrated that pharmacological inhibition of NK1R effectively reduces the growth of several tumor types such as NB [3,4].

In recent years, our research group has developed a library of carbohydrate-based Aprepitant analogs and conducted its evaluation as anticancer agents against a wide range of cancer cell lines. All the prepared compounds, derived from either D-galactose or L-arabinose, showed high NK1R affinity and antagonistic activity of SP, with broad-spectrum anticancer activity and an important selectivity, comparable to Cisplatin (Fig. 1) [7].

Considering these good results, in the present work, we address the determination of the selective cytotoxic activity of D-galactose and L-arabinose-derived NK1R antagonists for the treatment of NB. Furthermore, we describe the design and the stereoselective synthesis of a novel generation of nitrogenous D-glucose derivatives as analogs of Aprepitant (Fig. 1).

2. Results and discussion

2.1. Biological evaluation

2.1.1. NK1R expression vs prognosis in neuroblastoma patients

In order to investigate the potential association between NK1R expression and prognosis in neuroblastoma, we initially analyzed a publicly available gene expression dataset comprising 88 neuroblastoma tumors [8]. Patients were clustered in two groups (high *vs* low NK1R expression) and survival probability was evaluated by Kaplan-Meier curves. We found a significantly lower overall survival and relapse free survival probability in high NK1R expression group compared to low expression group (Fig. 4A). Moreover, we also found a similar result when we evaluate the survival probability of high-risk patients (stage 4, and age >18 months) in the same dataset (Fig. 4B).

Next, full-length tachykinin receptor 1 fl-NK1R and truncated tr-NK1R mRNA expression were examined in a panel of NB cell lines and the non-tumoral cell line RPE-1 using quantitative RT-PCR (Fig. 4C). Both spliced variants of NK1R were expressed in all human cell lines assessed, although expression levels varied between cell lines. Only the IMR32 cell line showed significantly higher fl-NK1R expression compared to the RPE-1 cell line. On the other hand, the expression of tr-NK1R was significantly higher in IMR32 and Kelly cell lines compared to the RPE-1 cell line. In general, while fl-NK1R exhibited a low expression profile, tr-NK1R showed much higher expression levels in all the assessed cell lines.

2.1.2. Cytotoxicity profiles

Considering the previous results, we selected Kelly and SH-SY5Y neuroblastoma cell lines to carry out the determination of anticancer activity of our D-galactose and L-arabinose-derived NK1R antagonists (Fig. 1) through MTT assays. Additionally, we tested these compounds on the non-tumor retinal pigmented epithelium cell line RPE-1. Cells were treated with increasing concentrations of compounds for 72 h and cell viability was evaluated, and half maximal inhibitory concentrations (IC_{50}) were calculated. Aprepitant was employed as a reference control to evaluate the activity of the new derivatives, as it is a known NK1R antagonist. The obtained results are collected in Table 1 (see Figure S1)

It should be noted that Kelly and SH-SY5Y exhibited a concentration-dependent decrease in cell viability in response to most derivatives, except for the hemiacetals **1(α,β)** and **5(α,β)** (Fig. 1) that showed little effect in the tested cell lines. As in previous studies, this result demonstrates that the trifluoromethyl substituent at the anomeric position is indispensable for the anticancer activity [9–11].

Protection of the hydroxyl groups at positions 3 and 4 of D-galactose derivatives increased the selective activity in **2α** and **2β**, with a significant increase in their cytotoxic activity (compare entries 2 and 3 *vs* entries 4 and 5, Table 1). Unlike the results obtained previously in solid tumor activity studies [7], the introduction of the 4,6-O-benzylidene acetal in both diastereomers, **3α** and **3β,** (entries 6 and 7, Table 1) resulted in a decrease in activity. Interestingly, in this case, the β-anomer exhibited a significant higher anticancer activity compared to the

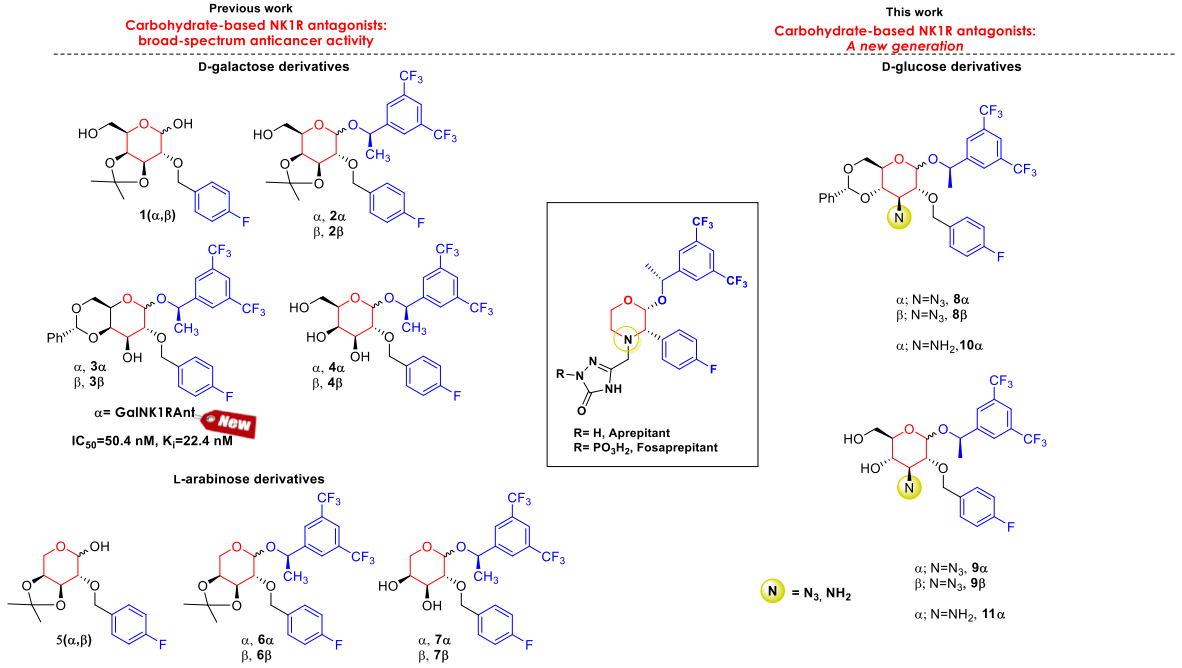

Fig. 1. NK1R antagonists derived from carbohydrates described in our previous work (left), structure of Aprepitant and Fosaprepitant (center), and new generation of nitrogenated D-glucose-based analogs of Aprepitant (right).

Table 1
IC_{50} Values of D-galactose and L-arabinose derivatives and Aprepitant on neuroblastoma cell lines (Kelly and SH-SY5Y) *vs* non-tumor cell line (RPE-1).

		IC_{50} (mean ± SEM; μM)			Selectivity index[a]	
Entry	Compound	Kelly	SH-SY5Y	RPE-1	RPE-1/ Kelly	RPE-1/ SH-SY5Y
1	**1(α,β)**	OR	OR	OR		
2	**2α**	**30.5 ± 6.9**	**28.4 ± 6.4**	**OR**		
3	**2β**	**24.8 ± 2.9**	**29.5 ± 3.0**	**OR**		
4	**4α**	37.4 ± 4.9	71.6 ± 13.9	28.4 ± 4.9	0.8 ± 0.2	2.5 ± 0.7
5	**4β**	47.4 ± 12.2	64.7 ± 2.7	25.8 ± 11.8	0.5 ± 0.3	2.5 ± 1.2
6	**3α**	**111.8 ± 70.0**	**127.5 ± 72.3**	**OR**		
7	**3β**	48.5 ± 1.5		251.0 ± 29.1	4.6 ± 0.1	
8	**5(α,β)**	OR	OR	OR		
9	**6β**	72.1 ± 20.6	117.0 ± 18.6	288.0 ± 12.4	4.0 ± 1.2	0.4 ± 0.1
10	**6α**	**42.9 ± 8.0**	**50.9 ± 8.9**	**OR**		
11	**7β**	**43.1 ± 3.1**	**46.5 ± 6.5**	**OR**		
12	**7α**	**27.0 ± 0.6**	**31.1 ± 4.9**	**OR**		
19	**Aprepitant**	15.1 ± 0.6		176.3 ± 38.8	11.7 ± 2.6	

OR: out of range (min. concentration for IC_{50} calculation not reached).
[a] The selectivity index is the mean of the selectivity indices calculated in each individual experiment. The selectivity index is calculated by dividing the IC_{50} value obtained in the nonmalignant cell line (RPE-1) by that in the cancer cell line (Kelly and SH-SY5Y). The most selective compounds are shown in bold.

α-anomer.

L-Arabinose derivatives **6β-7α** also exhibited high selective anticancer activity. In this case, deprotection of the hydroxyl groups at 3 and 4 positions increased the anticancer activity, with α-anomers (**6α** and **7α**) being more active than β-anomers (**6β** and **7β**) (compare entry 10 *vs* 9 and entry 12 *vs* 11).

Summing up, **2β** and **7α** were more cytotoxic against Kelly than the other derivatives, and like Fosaprepitant, a prodrug of Aprepitant, against SH-SY5Y (IC_{50}: 21.09 μM) [6]. Noteworthy, both of these carbohydrate derivatives showed higher selectivity than Aprepitant. Consequently, **2β** and **7α**, along with their respective anomers (**2α** and **7β**), whose cytotoxic profile is indicated in Fig. 5, were selected for further investigation into their cellular effects, specifically in relation to cell cycle regulation and apoptosis in neuroblastoma.

2.1.3. Cellular responses

The effect of selected carbohydrate derivatives, **2α**, **2β**, **7β**, **7α**, was analyzed on cell cycle and apoptosis in neuroblastoma cells to compare its cellular effects. As shown in Fig. 6A, we observed a significant pro-apoptotic effect of **2α**, as treated cells efficiently increased the early (Annexin V+/7AAD-) apoptotic population at a concentration lower than its IC_{50} values. This effect was like that observed when the cells were treated with Aprepitant. **2β**, **7β** and **7α** were also assayed at a concentration close to their IC_{50} value, but non-significative effect was observed.

When the effect of carbohydrate derivatives on cell cycle was evaluated, we detected a significant arrest in S phase in **2α** treated cells; this increase in the percentage of cells in S phase was concomitant with a decrease in the percentage of cells that achieved the G2/M phase. The effect of Aprepitant was similar to that observed for **2α** (Fig. 6B).

2.2. Docking calculations

Taking into account these biological results and the previously determined broad-spectrum anticancer activity against solid tumors, we considered the possibility of preparing glycosyl derivatives with a nitrogenated group instead of a hydroxyl group at the 3-position of the pyranose ring. Specifically, we decided to introduce an azide group because its reduction to an amino group at the C-3 position imparts a greater structural similarity to this new analog compared to Aprepitant, which features an amine-type nitrogen in the morpholine ring. In addition, the versatility of the azido group allows for its transformation into various functional groups, enabling the creation of a wide range of organic compounds as Aprepitant analogs. In order to explore the intermolecular interactions of these novel compounds within NK1R we performed molecular docking calculations.

The docking studies conducted with the newly design D-glucose derivatives and the NK1R showed that, similar to the NK1R antagonists, L-arabinose and D-galactose derivatives and Aprepitant [7], the hydrophobic 1,3-bis(trifluoromethyl)benzene and 4-fluoromethylbenzene fragments establish π-π stacking, π-alkyl, and alkyl-alkyl interactions within the innermost part of the binding site. These interactions predominantly occur with hydrophobic or amphipathic residues (Ala294, Ile113, Ile116, Ile204, Met81, Met291, Met295, Phe110, Phe111, Phe264, Trp261, Val200), in accordance with the principle of complementarity of hydrophobic patterns of the proteins and their docked ligands [12,13].

Furthermore, robust hydrogen bonds (<3.4 Å) have been observed between fluorine atoms of the 3,5-bis(trifluoromethyl)phenyl and *p*-fluorobenzyl fragments and the amino group of Asn89 and the hydroxyl group of Thr201, respectively. Additionally, fluorine bonds [14] with the carbonyl group of Pro112 have been detected, as depicted in Fig. 2 in the interaction diagrams. These fragments are in the same region of the binding site in all the synthesized antagonists (Figure S3).

The presence of the phenyl ring in the benzylidene moiety of **8α**, **8β**, **10α** and **10 β** causes the longitudinal molecular axis of these antagonists to be approximately 15 Å. This length allows them to interact with residues both in the central and outer parts of the binding site (Fig. 3). These interactions involve intense stabilizing π-π stacking, π-alkyl hydrophobic interactions and van der Waals interactions with residues such as Phe267, Phe268, Ile283, Tyr92, Tyr287 and Ala93 (Fig. 2). It is worthy to note that aromatic ring interactions have a key role in both drug design and protein-ligand recognition [15].

Therefore, the interactions of the phenyl ring of the acetalic fragment with the predominantly hydrophobic and amphiphilic residues in the outer part of the binding site enhance the electronic and steric complementarity of the ligands within the binding pocket, which boost the interaction with the receptor. Furthermore, the presence of a rotatable bond in the benzylidene moiety enables the phenyl ring to adopt diverse conformations within the binding site to optimize its interactions with the neighboring residues beyond those shown in the best docked poses (Fig. 3 and Figure S3). Regarding Aprepitant, the oxotriazol group is in a different region than the benzylidene group of the glucose analogs. In that region the only charged residue (Glu193) of the outer part of the binding site is located. Therefore, the oxotriazol fragment establishes a hydrogen bond with the carboxyl group of this residue, as well as with the amino group of Trp184. The relatively low hydrophobicity of this moiety (log P = −0.64) results in insufficient electronic complementarity in the region where the benzylidene group is located, which is predominantly characterized by hydrophobic and amphiphilic residues. Consequently, it is not capable of docking in that specific region.

The polar nature of $–NH_2$ and $–N_3$ groups at position 3 causes them to orient towards the outer region of the binding site, where the highest solvent accessibility is located. This orientation assists in minimizing the binding energy penalty linked to the displacement of water molecules from charged or polar groups [16,17].

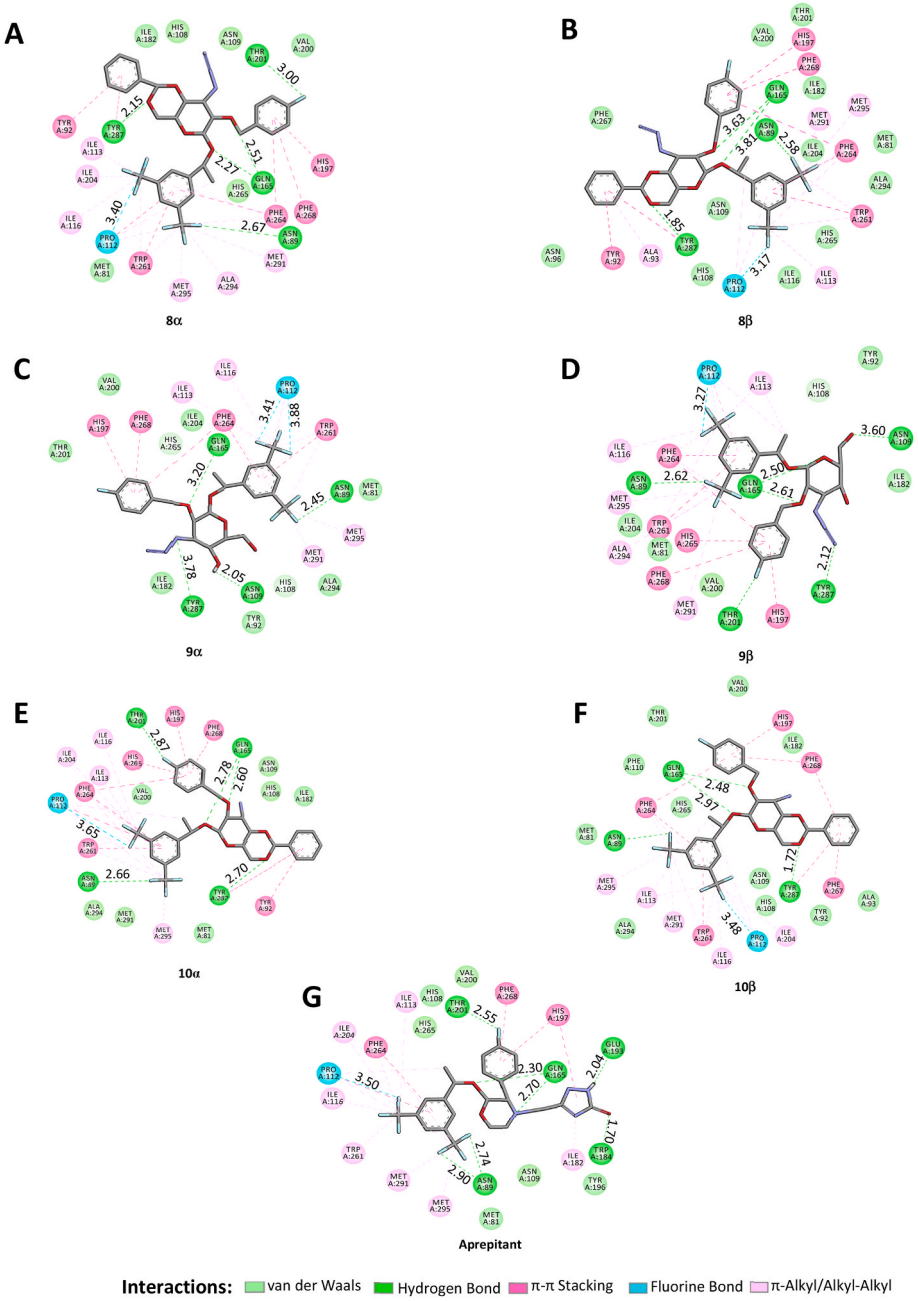

Fig. 2. Two-dimensional view of the interaction type for the best docked poses of **8α** (A), **8β** (B), **9α** (C), **9β** (D), **10α** (E) **10β** (F) and **Aprepitant (G)** with surrounding amino acids of NK1R (PDB ID: 6HLO). The distances for hydrogen bonds and fluorine bonds are given in Å.

One advantage of designing NK1 antagonists based on carbohydrates is that all oxygen atoms are in six-membered rings, which have low strain and a high capacity for puckering and deformation. This provides them with dynamic degrees of freedom to establish strong hydrogen bonding interactions with donor groups of Gln165 and Asn109 residues in the central part, and Tyr287 residue in the outer part of the binding site (Fig. 2). On the other hand, morpholine fragment of Aprepitant, located at the same region than D-glucose moieties, only interact with Gln165 residue. Furthermore, as in the case of D-galactose and L-arabinose derivatives, the moderate hydrophobicity of the D-glucose ring, including the ether oxygens at 1 and 2 positions within the binding site center (logP = 0.53), results in no penalty for interaction with the hydrophobic residues Phe264 and Phe268 located in the central region of the binding site.

Finally, the docking score values of the studied ligands were −12.2 kcal/mol for **8α** and **10α**, −12.1 kcal/mol for **8β** and **10β**, −11.2 kcal/mol for Aprepitant and −9.9 and −9.2 kcal/mol for **9β** and **9α**, respectively. These results indicate that the incorporation of D-glucose and benzylidene fragments in the studied compounds yields better docking scores compared to those of morpholine and oxotriazol moieties present in Aprepitant. This improvement can be attributed to the enhanced flexibility and enlarged hydrophobic interactions facilitated by the former fragments. The obtained low docking scores for ligands **9β** and **9α** highlight the significance of the molecular fragments situated in the outer region of the binding site that allow to engage in an array of additional interactions with NK1R.

2.3. Chemistry

Encouraged by the results obtained in the docking studies, we

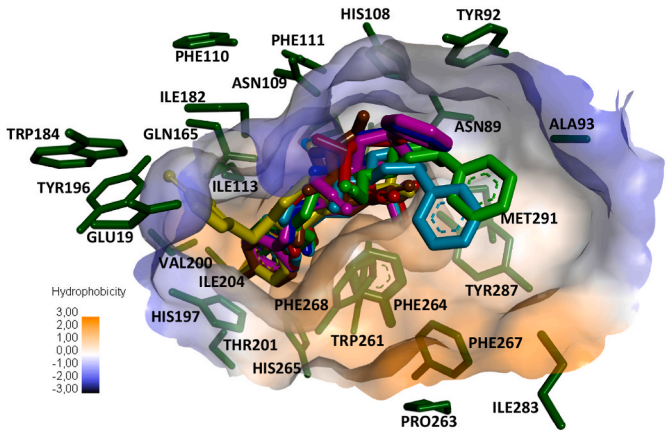

Fig. 3. Binding site residues of NK1R (dark green), hydrophobicity surface and best docked poses for: **8α** (magenta), **8β** (green), **9α** (red), **9β** (brown) **10α** (dark blue) **10β** (bright blue) and **Aprepitant** (yellow). For clarity, hydrogen atoms have been removed. Orange colour represents the most hydrophobic surface area; blue colour represents the least hydrophobic.

designed a new generation of D-glucose-based analogs of Aprepitant, starting from diaceton-D-glucosa (DAG), a commercial, low-cost D-glucose furanose derivative. The utilization of this carbohydrate could potentially enhance its structural recognition by active transport agents, thereby facilitating more efficient passage across specific membranes and ultimately achieving greater activity. Moreover, this represents a simple and economical alternative to access biocompatible heterocyclic compounds with multiple chiral centers in proximity. From the chiral pool, carbohydrates can be considered the best-suited family for this purpose, as stereochemically rich compounds with hydroxyl groups in virtually all arrangements, allowing easy tuning of their steric, electronic, and three-dimensional (3D) structures. Furthermore, being plentiful and renewable biomolecules, they are readily available on a large scale at a low cost. In fact, certain monosaccharides are more affordable than the commonly used solvents in synthetic laboratories.

2.3.1. *Synthesis of D-glucose-derived NK1R antagonists (GlucoNK1RAnt)*

The oxidation of DAG with P_2O_5 in DMSO, followed by reduction with $NaBH_4$, resulted in the C-3 epimer **12** (75% yield) with *allo* configuration [18,19] which by subsequent treatment with Tf_2O produced the relative unstable triflate **13**. It was directly reacted with NaN_3 leading to the azide **14** with a quantitative yield and inversion of the configuration at C-3 (Scheme 1) [20,21].

The corresponding peracetylated glucopyranose derivative **15(α,β)**

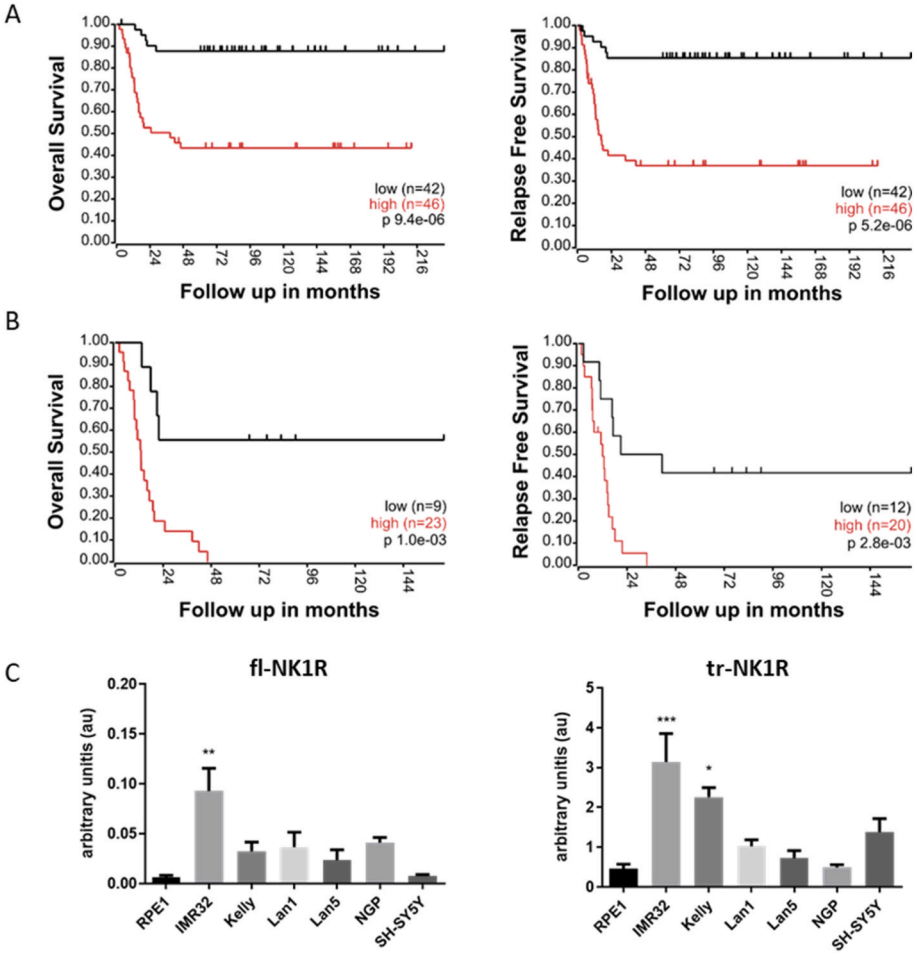

Fig. 4. NK1R expression and survival in neuroblastoma. Kaplan-Meier curves show OS and RFS of neuroblastoma patients stratified by NK1R expression. Plots are relative to (A) all patients included in this dataset, and (B) high-risk patients (stage 4, and age >18 months). Curves were compared by log-rank test and the p-value is reported (black-low expression and red-high expression; number of patients of each group is indicated for each graph). OS: Overall survival; RFS: Relapse-free survival. C) Quantitative RT-PCR of full-length tachykinin receptor 1 fl-NK1R and truncated tr-NK1R mRNA in a panel of neuroblastoma cell lines and the non-tumoral cell line RPE1. Data are presented as mean ± SEM (n = 3), *p < 0.05, **p < 0.005, ***p < 0.0005 significant differences compared to RPE1 cells evaluated by one-way ANOVA test, followed by a Bonferroni post-hoc test.

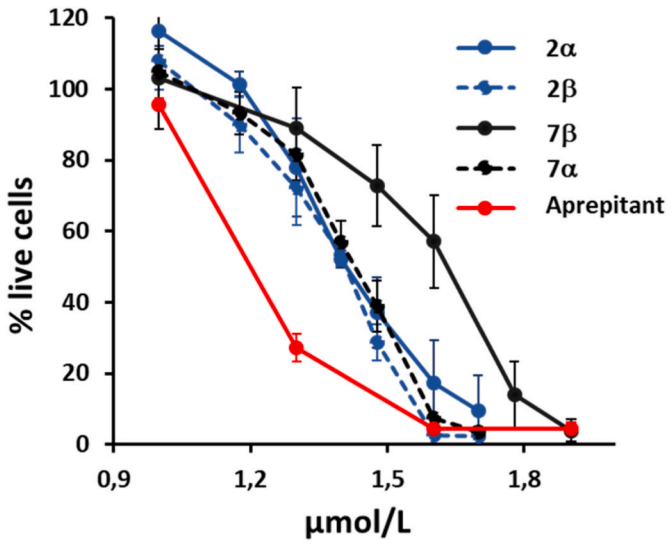

Fig. 5. Cytotoxicity profile of selected Aprepitant analogs. MTT assays of Kelly cells treated with increasing concentrations of **2α**, **2β**, **7β**, **7α** and Aprepitant. Results are expressed as a percentage of live cells with respect to control cells in the absence of the compound (72 h; mean ± SEM, n = 3 independent experiments).

was obtained with high yield (74% yield) through the acid hydrolysis of **14**, followed by acetylation [22]. The thioglycosylation of **15(α,β)** resulted in the peracetylated phenylthioglycoside **16(α,β)** with a 77% yield [22]. In this case, unlike previous studies with D-galactose and L-arabinose derivatives [23], where thioglycosylation occurred efficiently at room temperature, we had to raise the temperature to ensure the completion of the reaction [22]. Deacetylation of **16(α,β)** under Zemplen conditions quantitatively yielded the trihydroxylated derivative **17(α,β)** (Scheme 1) [23]. Next, the corresponding benzylidene acetal was formed, and the installation of the *p*-fluorophenyl fragment was carried out in THF, using NaH and *p*-fluorobenzyl chloride (Scheme 1) [23].

The application of Schmidt trichloroacetimidate methodology for glycosylation of compound **20(α,β)** resulted in a complex mixture [23]. Fortunately, the direct glycosylation of phenylthioglycoside **20(α,β)** with NIS and alcohol **(*R*)-21** gave the corresponding glycosides **8α** and **8β** (43% yield), in a 5:1 ratio, (Scheme 2). Contrary to the earlier conducted thioglycosylation of L-arabinose [7], the use of TMSOTf as an acid catalyst was essential for facilitating the glycosylation reaction of D-glucose derivative **20(α,β)**. Regarding the addition of NIS, both the yield and the α:β ratio of glycosides obtained were higher when it was carried out in a single step rather than in two portions (43% yield *vs* 34% yield and α:β ratio of 1:0.2 and 1:0.4, respectively).

The predictable equatorial position of the phenyl group in the benzylidene acetal for thioglicosides **8α** y **8β** was validated by ^{1}H NMR NOE experiments (see the Supporting Information).

Deprotection of the hydroxylic groups at 4 and 6 positions in both anomers, **8α** and **8β** (Scheme 2) allowed us to modulate lipophilicity and investigate the structure-activity relationship. Thus, acid hydrolysis of the benzylidene acetal with CSA in methanol, yielded the corresponding dihydroxy derivatives **9α** and **9β**, in 61% and 60% yields respectively (Scheme 2) [23].

Given the low yield (7%) obtained from the β-anomeric form in the glycosylation, we exclusively utilized the α-anomer for the final steps of the synthesis. The reduction of the azide group with $LiAlH_4$ in THF led to the corresponding amine derivative **10α** and **11α** with a 67% and a 58 % yields respectively (Scheme 3).

To determine the antitumor selective activity of this new series of D-glucose derivatives, we performed MTT assays in Kelly and RPE-1 cell lines, following the same procedures previously employed for D-galactose and L-arabinose derivatives (see 2.1.2 section). The obtained results are collected in Table 2 (see Figure S2).

Regarding the new D-glucose derivatives, we observed that, like L-arabinose and D-galactose derivatives, the β anomers showed the most

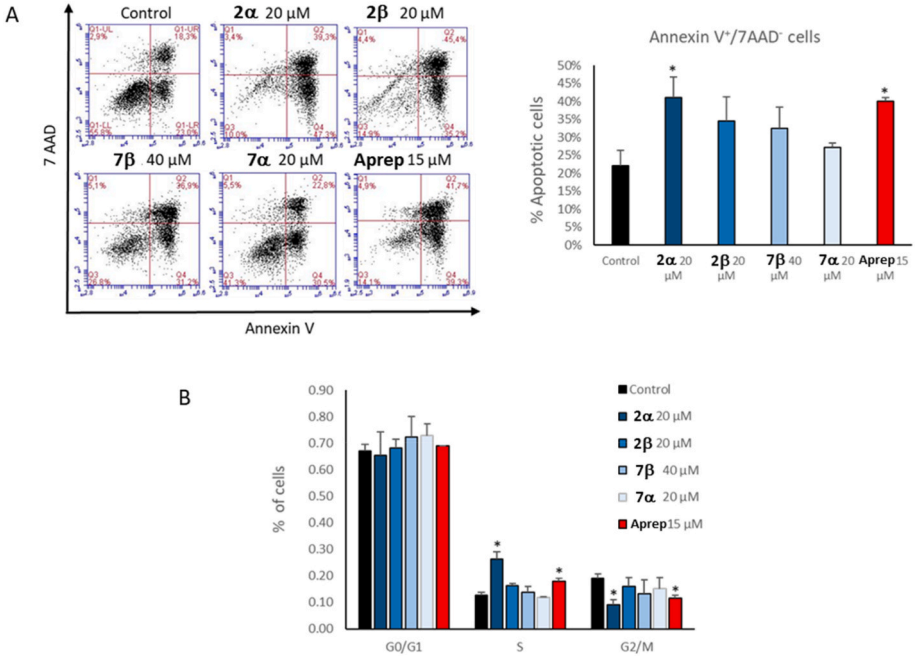

Fig. 6. Cellular responses of Kelly cells treated with **2α**, **2β**, **7β**, **7α** and Aprepitant. Top: representative flow cytometry dot plots for Annexin V and 7AAD staining of Kelly cells treated with Aprepitant (15 µM) and carbohydrate derivatives (20 µM or 40 µM) for 48h. Numbers depict the percentage of cells in each phase. Q1-Necrotic (dead) cells; Q2- Late apoptotic cells; Q3- Viable cells; Q4- Early apoptotic cells. Bottom: A) Quantification of early apoptotic annexin-V+/7AAD-cells for each treatment (mean ± SEM, n = 3 experiments). B) Quantification of cell cycle phases (G0/G1, S and G2/M) of Kelly cells treated with Aprepitant and carbohydrate derivatives for 48h (mean ± SEM, n = 3 experiments). (*p < 0.05 *vs* control).

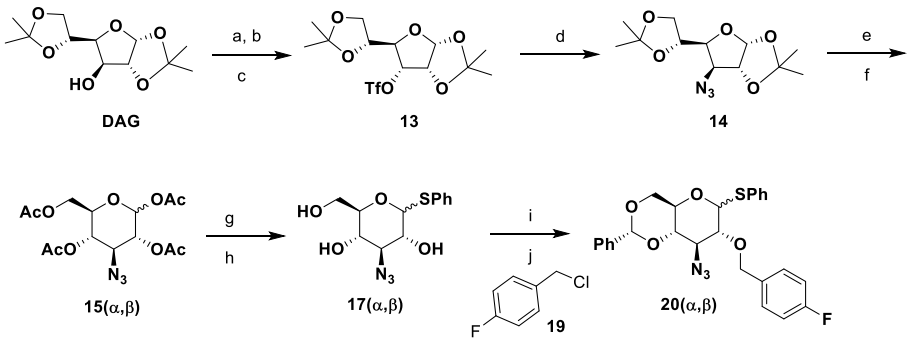

Scheme 1. Synthesis of *p*-fluorobenzyl D-glucose derivative **20(α,β)**. Reagents and conditions: (a) P_2O_5, dimethylsulfoxide (DMSO), 50 °C; (b) $NaBH_4$, H_2O, *tert*-butyl methyl ether (TBME), 0 °C–10 °C; (c) Tf_2O, CH_2Cl_2: pyridine (10:1), 0 °C (quant. yield); (d) NaN_3, dimethylformamide (DMF), rt (quant. yield); (e) CF_3COOH:H_2O (20:3), 0 °C; (f) Ac_2O, pyridine, rt, α:β 1:0.7 (74% yield); (g); Ph-SH, $BF_3{\cdot}Et_2O$, CH_2Cl_2, 40 °C, α:β 0.2:1; (h) $NaOCH_3$, MeOH, rt, α:β 0.1:1 (77% yield); (i) $PhCH(OCH_3)_2$, 10-camforsulfonic acid (CSA), DMF, rotavapor, 35 °C, α:β 1:10; (j) NaH, NBu_4, **19**, THF, rt, α:β 1:10 (quant. yield).

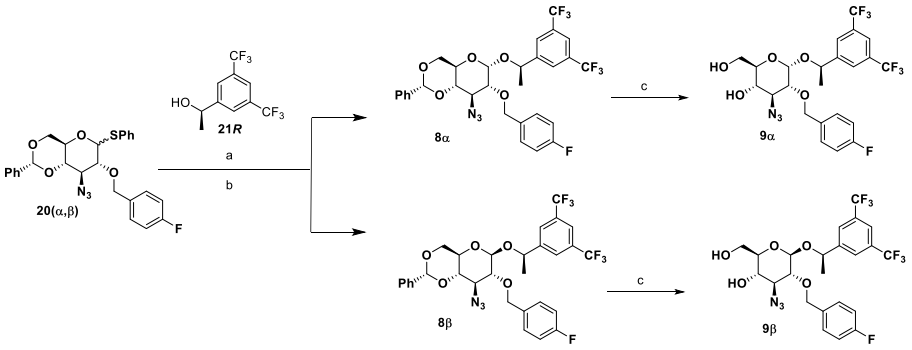

Scheme 2. Synthesis of D-glucose derivatives **8α**, **8β**, **9α** and **9β**. Reagents and conditions: (a) (*R*)-1-[3,5-bis(trifluoromethyl)phenyl]ethan-1-ol (**21*R***), NIS, CH_2Cl_2, TMSOTf, 4 Å molecular sieve (MS), rt, darkness; (b) column chromatography: α:β 5:1 (36% and 7% yield respectively); (c) CSA (cat), MeOH, rt (61% yield **9α** and 80% yield **9β**).

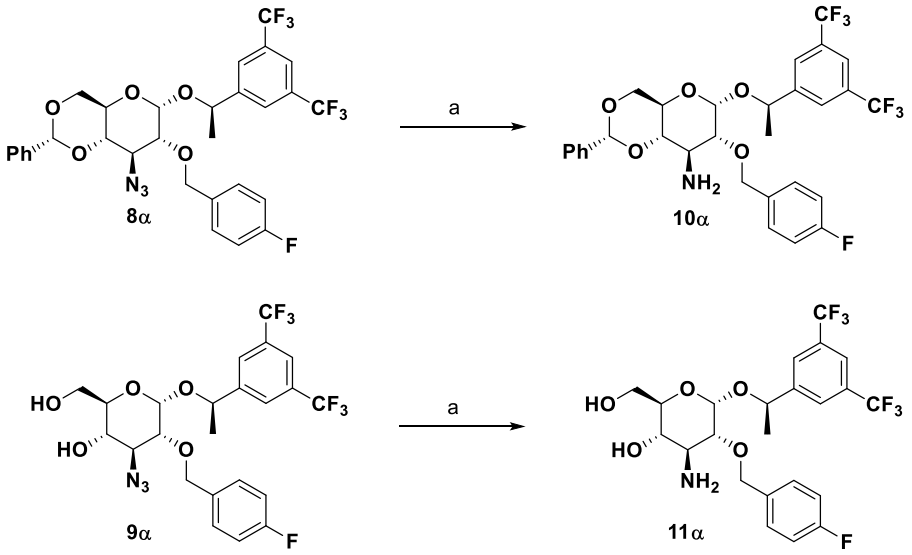

Scheme 3. Synthesis of amine derivatives **10α** and **11α**. Reagents and conditions: (a) $LiAlH_4$, THF, rt (67% yield **10α** and 58% yield **11α**).

potent activity against the Kelly cell line. This suggests that Aprepitant analogs based on carbohydrates have improved anticancer effects when the 3,5-bis(trifluoromethyl)benzyl fragment is in the equatorial position, opposite to that of the acetal carbon in the Aprepitant's eutomer. Introducing the N_3 group at position 3 in D-glucose derivatives (along with the change in configuration at C-4) significantly enhances selectivity compared to D-galactose derivatives **4α** and **4β** (compare entries 4 and 5, Table 1 *vs* 3 and 4, Table 2). Additionally, compound **9β** showed superior anticancer activity compared to the β-D-galactose analog **4β** (entries 5, Table 1 *vs* 4, Table 2), and exhibited similar IC_{50} values but significantly higher selectivity than Aprepitant.

Docking studies showed that the solvated amino group is positioned

Table 2
IC_{50} Values of D-glucose derivatives on neuroblastoma cell line Kelly *versus* non-tumor cell line (RPE-1).

		IC_{50} (mean ± SEM; μM)		Selectivity index[a]
Entry	Compound	Kelly	RPE-1	RPE-1/Kelly
1	**8α**	**234.4 ± 70.4**	**OR**	
2	**8β**	**107.4 ± 3.8**	**OR**	
3	**9α**	**88.4 ± 26.0**	**OR**	
4	**9β**	**16.8 ± 0.8**	**OR**	
5	**10α**	**6.3 ± 0.5**	**92.3 ± 7.6**	**14.7 ± 1.7**
6	**11α**	33.6 ± 4.7	145.7 ± 10.0	4.3 ± 0.7
	Aprepitant	15.1 ± 0.6	176.3 ± 38.8	11.7 ± 2.6

OR: out of range (min. concentration for IC_{50} calculation not reached).
[a] The selectivity index is the mean of the selectivity indices calculated in each individual experiment. The selectivity index is calculated by dividing the IC_{50} value obtained in the nonmalignant cell line (RPE-1) by that in the cancer cell line (Kelly). The most selective compounds are shown in bold.

similarly to N_3 outside the binding site. These amino derivatives displayed markedly enhanced anticancer activity, surpassing Aprepitant, especially **10α**. This indicates that OH interactions at C-3 might not be essential for the anticancer effect. While the amino group could reduce cytotoxic selectivity, these derivatives still maintain selectivity, even more than Aprepitant, particularly **10α**.

In summary, nine of the tested carbohydrate-based derivatives (**2α, 2β, 3α, 6α, 7α, 7β, 8α, 8β,** and **9α**) exhibit complete selective cytotoxic activity against neuroblastoma *in vitro*. This represents an outstanding foundation for upcoming *in vivo* assays, where a wide therapeutic range can be expected for these products.

Although some of them (**3α, 8α, 8β**, and **9α**) have an IC_{50} greater than 50 μM, they remain potential candidates for treating this disease. Given the role of NK1R in processes like pain, anxiety, and depression, NK1 antagonists usually have few side effects and often provide beneficial health outcomes [24].

3. Conclusions

To summarize, we have reported the evaluation of carbohydrate-based derivatives as potential Aprepitant analogs for neuroblastoma treatment. We explored D-galactose and L-arabinose derivatives, known for their broad-spectrum anticancer properties and high selectivity. The docking calculations of a new family of D-glucose derivatives confirms the importance of pyranose and benzylidene fragments on the establishment of new intermolecular interactions in order to improve the molecular recognition process with NK1R.

Specifically, the galactosyl derivative **2α** emerged as a promising candidate, displaying substantial *in vitro* cytotoxic activity against NB (IC50 = 30.5 ± 6.9 μM). Its IC_{50} value falls within the range of Aprepitant and its prodrug Fosaprepitant, indicating a similar apoptotic effect as Aprepitant but with significantly higher selectivity.

Notably, most analogs exhibited remarkable selective cytotoxic activity against neuroblastoma cell lines, surpassing that of Aprepitant. Nevertheless, incorporating an amino group at position 3 of the glucose ring notably boosted anticancer activity, albeit at the expense of reduced selectivity. Among all the tested analogs, the amino derivative **10α** particularly excelled, displaying superior *in vitro* cytotoxic activity against neuroblastoma (IC_{50} = 6.3 ± 0.5 μM) compared to Aprepitant (IC_{50} = 15.1 ± 0.6 μM), making it 1.2 times more selective.

These findings highlight the potential of these carbohydrate-based derivatives, especially **2α** and **10α**, as promising candidates for neuroblastoma therapy.

It is important to highlight that the utilization of carbohydrate derivatives may potentially improve their structural recognition by active transport agents, thereby promoting more efficient passage across specific membranes and ultimately leading to increase *in vivo* activity.

4. Experimental section

4.1. Synthesis

General Procedures. The monitoring of the reactions was carried out by thin layer chromatography using silica gel chromatographs type 60F25H with a layer thickness of 0.2 mm (Merck). The plates have been analyzed in a 254/365 nm UV lamp and developed with phosphomolybdic acid, sulfuric acid and ninhydrin. The purification and separation of the reaction products were carried out by column chromatography under pressure (flash chromatography), using type 60 silica gel as the stationary phase, with a particle size of 35–70 μm. In each specific case, the eluents used as mobile phase and the proportions of solvents in v/v have been indicated.

In the cases in which it has been indicated that the reaction has taken place under an inert atmosphere, glassware previously dried in an oven and anhydrous solvents have been used. The solvents have been dried with a 4 Å molecular sieve, previously activated in microwaves and under vacuum.

The NMR spectra have been carried out at room temperature, indicating the solvent used in each case. The ^1H NMR and ^{13}C NMR spectra have been recorded on the Bruker DRX-500 devices of the Nuclear Magnetic Resonance Service of the University of Seville. In each case, the chemical shifts have been indicated on the δ (ppm) scale, referring to the solvent used, the number of protons calculated by integration and the value of the coupling constants J (Hz).

The mass spectra have been recorded on a Kratos EM-80RFA 241 MC spectrometer using electronic impact or FAB techniques, by the Mass Spectrometry service of the University of Seville.

The optical rotations $[\alpha]_{20}^{D}$ have been determined at room temperature in a PerkinElmer 341 MC polarimeter, using sodium yellow light (λ = 589 nm) and cells of 1 dm length. In each case, the solvent used has been indicated, as well as the concentration (c in g/100 mL). Melting points have been determined on a Gallemkamp apparatus in open capillary tubes.

1,2,5,6-O-isopropylidene-D-allofuranose, (12). To 25 mL of DMSO under argon atmosphere and at 18–20 °C, P_2O_5 (5.5 g, 38.40 mmol) was slowly added. After stirring for 15 min at 18–20 °C, a solution of diacetone-D-glucose (10.0 g, 38.40 mmol) in 50 mL of DMSO was added. The mixture was then heated at 50 °C until the starting product was consumed (3 h). Next, after adding TBME (60 mL) to the mixture, both phases were separated, and the aqueous phase was extracted with TBME (40 mL). The combined organic phases were evaporated under reduced pressure to a volume of 75 mL and added, at 0–10 °C, to a solution of 0.9 g of $NaBH_4$ (24.20 mmol) in distilled H_2O (38 mL). After stirring for 30 min, the reaction mixture was diluted with distilled H_2O (40 mL), both phases were separated, the aqueous phase was extracted with CH_2Cl_2 (3 x 40 mL), and the combined organic phases were evaporated under reduced pressure. The obtained crude was dissolved in TBME (75 mL) and extracted with distilled H_2O (3 x 30 mL). The combined aqueous phases were extracted with CH_2Cl_2 (5 x 40 mL) and the organic extracts were dried over anhydrous Na_2SO_4. The solvent was evaporated under reduced pressure to obtain 9.9 g of **12** (38.11 mmol quant. yield) as a white solid. Mp: 76–78 °C. ^1H NMR (500 MHz, $CDCl_3$): δ 5.81 (d, J = 3.8 Hz, 1H, H_1), 4.61 (dd, J = 3.9 and 5.1 Hz, 1H, H_4), 4.30 (td, J = 4.8 and 6.6 Hz, 1H, H_5), 4.10-3.99 (m, 3H, H_2, H_6, $H_{6'}$), 3.82 (dd, J = 4.8 and 8.5 Hz, 1H, H_3), 2.52 (d, J = 8.4 Hz, 1H, OH), 1.58 (s, 3H, CH_3), 1.46 (s, 3H, CH_3), 1.38 (s, 3H, CH_3), 1.37 (s, 3H, CH_3) ppm. ^{13}C NMR (125 MHz, $CDCl_3$): δ 113.0, 110.0, 104.1, 80.0, 79.2, 75.8, 72.7, 66.1, 26.7, 26.7, 26.5, 25.4 ppm. HRMS: calcd for $C_{12}H_{20}O_6Na$ $[M+Na]^+$: 283.1152; found 283.1156 (0.3935 ppm).

3-Deoxy-1,2,5,6-O-isopropylidene-3-azido-α-D-glucofuranose, (13). To a solution of 5.0 g of 1,2,5,6-O-Isopropylidene-α-D-allofuranose (19.21 mmol) in 55 mL of a CH_2Cl_2:Pyridine 10:1 mixture, under argon atmosphere and at 0 °C, 4.8 mL of trifluoromethanesulfonic anhydride (28.81 mmol) was added dropwise. After stirring for 30 min, the starting

product was consumed, and the reaction mixture was quenched with distilled H_2O. The aqueous phase was extracted with CH_2Cl_2 (3 x 50 mL) and the combined organic phases were washed with saturated NaCl solution (1 x 30 mL), dried over anhydrous Na_2SO_4 and filtered. The solvent was evaporated under reduced pressure. To a solution of the obtained triflate in 200 mL of DMF, 5.8 g of NaN_3 (88.83 mmol) was added at 0 °C and the temperature was allowed to rise to room temperature. Once the starting product was consumed (24 h), the reaction was quenched with distilled H_2O and the solvent was evaporated under reduced pressure. The residue was dissolved in saturated NaCl solution and extracted with CH_2Cl_2 (3 x 50 mL). The combined organic phases were washed with saturated NaCl solution (1 x 30 mL), dried over anhydrous Na_2SO_4, filtered, and the solvent was evaporated under reduced pressure to obtain 5.1 g of **13** (17.73 mmol quant. yield) as an orange syrup. ^{1}H NMR (500 MHz, $CDCl_3$): δ 5.85 (d, J = 3.6 Hz, 1H, H_1), 4.61 (d, J = 3.6 Hz, 1H, H_4), 4.26-4.21 (m, 1H, H_5), 4.15-4.08 (m, 3H, H2, H_6 and $H_{6'}$), 3.97 (dd, J = 8.7 and 4.9 Hz, 1H, H_3), 1.51 (s, 3H, CH_3), 1.43 (s, 3H, CH_3), 1.37 (s, 3H, CH_3), 1.32 (s, 3H, CH_3) ppm. ^{13}C NMR (125 MHz, $CDCl_3$): δ 112.5, 109.7, 105.2, 83.6, 80.7, 73.2, 67.8, 66.6, 27.0, 26.8, 26.4, 25.3 ppm. HRMS: Calcd for $C_{12}H_{19}O_5N_3Na$ $[M+Na]^+$: 308.1217; found 308.1219 (0.7 ppm).

3-Azido-3-deoxy-α,β-D-glucopyranose tetraacetate, (15(α,β)). 5.0 g of 3-Deoxy-1,2,5,6-O-isopropylidene-3-azido-α-D-glucofuranose (17.70 mmol) were dissolved in 43 mL of a mixture of CF_3COOH:H_2O 20:3 at 0 °C. After stirring for 1 h, the starting product was consumed, and the solvent was evaporated under reduced pressure. To a solution of the crude in 150 mL of pyridine under argon atmosphere and at 0 °C, 81.7 mL of acetic anhydride (864.80 mmol) were added, and the temperature was allowed to rise to room temperature. After stirring for 18 h, the reaction was quenched with ice-water and this mixture was extracted with CH_2Cl_2 (3 x 30 mL). Next, the organic phase was washed with 2 M H_2SO_4 solution (3 x 30 mL), saturated $NaHCO_3$ solution (3 x 20 mL) and saturated NaCl solution (1 x 20 mL). The mixture was dried over anhydrous Na_2SO_4, filtered and the solvent was evaporated under reduced pressure. The crude was purified by flash column chromatography (hexane/AcOEt 5:1) to obtain 4.86 g of **15(α,β)** (13.00 mmol, 74% yield) as a mixture of the two possible α:β anomers in a 1: 0.7 ratio, as a yellow oil. ^{1}H NMR (500 MHz, $CDCl_3$): δ 6.29 (d, J = 3.6 Hz, 1Hα, H_1), 5.66 (d, J = 8.3 Hz, 1Hβ, H_1), 5.05-4,98 (m, 1Hα, H_6, 2Hβ, H_6 and $H_{6'}$), 4.94 (dd, J = 3.6 and 10.7 Hz, 1Hα, $H_{6'}$), 4.25-4.18 (m, 1Hα, H_4, 1Hβ, H_4), 4.08 (td, J = 2.1 and 13.0 Hz, 1Hα,H_5), 4.06-4.00 (m, 1Hα, H_2, 1Hβ, H_2), 3.95 (t, J = 10.3 Hz, 1Hα, H_3), 3.78 (ddd, J = 2.3, 4.7 and 9.9 Hz 1Hβ, H_5), 3.68 (t, J = 10.1 Hz, 1Hβ, H_3), 2.17 (s, 3Hα, CH_3), 2.13 (s, 3Hα, CH_3), 2.12 (s, 3Hβ, CH_3), 2.11 (s, 3Hβ, CH_3), 2.10 (s, 3Hβ, CH_3), 2.09-2.06 (m, 6Hα, 3Hβ, CH_3) ppm. ^{13}C NMR (125 MHz, $CDCl_3$): δ 170.7, 170.7, 169.5, 169.2, 169.2, 169.1, 169.0, 168.7, 92.1, 88.9, 73.7, 70.3, 70.2, 70.1, 68.0, 68.0, 64.4, 61.7, 61.6, 61.0, 20.9, 20.9, 20.8, 20.7, 20.7, 20.6 ppm. HRMS: Calcd for $C_{14}H_{19}O_9N_3Na$ $[M+Na]^+$: 396.1014; found 396.1008 (−1.3 ppm).

Phenyl 2,4,6-tri-O-acetyl-3-azido-1,3-dideoxy-1-thio-D-glucopyranoside, (16(α,β)). To a solution of 3.3 g of 3-azido-3-deoxy-α,β-D-glucopyranose tetraacetate (8.80 mmol) and 1.8 mL of thiophenol (17.7 mmol) in 25 mL of CH_2Cl_2, under argon atmosphere and at room temperature, 4.5 mL of boron trifluoride etherate were added dropwise and left stirring at 40 °C. Once the starting product was consumed, after 17 h, the reaction mixture was treated with saturated $NaHCO_3$ (30 mL) solution. The aqueous phase was extracted with CH_2Cl_2 (2 x 40 mL) and the combined organic phases were washed with saturated NaCl (1 x 30 mL) solution, dried over anhydrous Na_2SO_4 and the solvent was evaporated under reduced pressure. In this way, an orange solid was obtained as a mixture of the two α:β anomers in a 0.2:1 ratio. After purification by flash column chromatography (hexane:AcOEt 7:1), 0.416 g of anomer **16α** (1.10 mmol, 11 % yield) as a brown solid and 2.4 g of anomer **16β** (5.60 mmol, 64 % yield) as a white solid were obtained.

Phenyl 2,4,6-tri-O-acetyl-3-azido-1,2-dideoxy-1-thio-β-D-glucopyranoside, (16β). ^{1}H NMR (500 MHz, $CDCl_3$): δ 7.51–7.49 (m, 2H, SC_6H_5), 7.33–7.30 (m, 3H, SC_6H_5), 4.93 (t, J = 10.0 Hz, 1H, H_2), 4.91 (t, J = 9.9 Hz, 1H, H_4), 4.66 (d, J = 9.9 Hz, 1H, H_1), 4.21–4.14 (m, 2H, H_6, $H_{6'}$), 3.69–3.64 (m, 2H, H_5, H_3), 2.18 (s, 3H, –$COOCH_3$), 2.12 (s, 3H, –$COOCH_3$), 2.08 (s, 3H, –$COOCH_3$) ppm. ^{13}C NMR (125 MHz, $CDCl_3$): δ 170.7, 169.3, 169.2, 133.1, 132.1, 129.1, 128.5, 86.5, 76.6, 70.2, 68.5, 66.0, 62.4, 20.9, 20.8, 20.7 ppm. HRMS: Calcd for $C_{18}H_{21}O_7N_3NaS$ $[M+Na]^+$: 446.0992; found 446.0987 (−1,3 ppm). M.p.: 117–119 °C. $[\alpha]_D^{20}$: 18,2 (c 1, $CHCl_3$)

Phenyl 2,4,6-tri-O-acetyl-3-azido-1,2-dideoxy-1-thio-α-D-glucopyranoside, (16α). ^{1}H NMR (500 MHz, $CDCl_3$): δ 7.44–7.42 (m, 2H, SC_6H_5), 7.33–7.28 (m, 3H, SC_6H_5), 5.89 (d, J = 5.6 Hz, 1H, H_1), 4.96 (dd, J = 5.4 and 10.6 Hz, 1H, H_2), 4.95 (t, J = 9.9 Hz, 1H, H_4), 4.49 (ddd, J = 2.3, 5.3 and 10.1 Hz, 1H, H_5), 4.22 (dd, J = 5.4 and 12.4 Hz, 1H, H_6), 4.02 (dd, J = 2.3 and 12.4 Hz, 1H, $H_{6'}$), 3.94 (t, J = 10.3 Hz, 1H, H_3), 2.18 (s, 3H, –$COOCH_3$), 2.15 (s, 3H, –$COOCH_3$), 2.01 (s, 3H, –$COOCH_3$) ppm. ^{13}C NMR (125 MHz, $CDCl_3$): δ 170.7, 169.7, 169.4, 132.3, 132.1, 129.4, 128.1, 85.1, 71.9, 68.6, 68.5, 62.1, 62.0, 20.9, 20.8 (2) ppm. HRMS: Calcd for $C_{18}H_{21}O_7N_3NaS$ $[M+Na]^+$: 446.0992; found 446.0987 (−1,6 ppm). M.p.: 125–127 °C. $[\alpha]_D^{20}$: +167,5 (c 1, $CHCl_3$).

Phenyl 3-azido-1,3-dideoxy-1-thio-D-glucopyranoside, (17(α,β)). To a solution of 5.9 g of the mixture of the two anomers **16α** and **16β** (13.90 mmol) in 70 mL of methanol, 0.01 g of sodium (0.50 mmol) was added, and the mixture was allowed to stir at room temperature. Once the starting product was consumed (24 h) the reaction was quenched with acid resin and filtered to obtain 4.0 g of a mixture of the two anomers **17α** and **17β** in a ratio of α:β 0.09:1 (13.60 mmol, quant. yield) as a brown solid.

Phenyl 3-azido-1,3-dideoxy-1-thio-α-D-glucopyranoside, (17α). ^{1}H NMR (500 MHz, DMSO-D_6): δ 7.50 (dd, J = 1.4 and 8.5 Hz, 2H, SC_6H_5), 7.32 (t, J = 7.4 Hz, 2H, SC_6H_5), 7.26 (tt, J = 1.1 and 7.3 Hz, 1H, SC_6H_5), 5.93 (d, J = 4.8 Hz, 1H, H_1), 5.57 (d, J = 6.9 Hz, 1H, OH), 5.52 (d, J = 5.3 Hz, 1H, OH), 4.54 (t, J = 5.9 Hz, 1H, $H_{6'}$), 3.89 (dt, J = 3.4 and 9.8 Hz, 1H, H_6), 3.69-3.64 (m, 1H, H_5), 3.56-3.52 (m, 2H, H_2, OH), 3.41 (t, J = 9.9 Hz, 1H, H_3), 3.28-3.23 (m, 1H, H_4) ppm. ^{13}C NMR (125 MHz, DMSO-D_6): δ 134.3, 131.3, 128.9, 126.8, 88.8, 73.6, 70.1, 67.9, 67.9, 60.0 ppm. HRMS: calcd for $C_{12}H_{15}O_4N_3NaS$ $[M+Na]^+$: 320.0675; found 320.0673 (−0.7034 ppm). Mp: 123–126 °C. $[\alpha]_D^{20}$: +294.3 (c 1, CH_3OH).

Phenyl 3-azido-1,3-dideoxy-1-thio-β-D-glucopyranoside, (17β). ^{1}H NMR (500 MHz, DMSO-D_6): δ 7.49, (d, J = 7.3 Hz, 2H, SC_6H_5), 7.34 (t, J = 7.6 Hz, 2H, SC_6H_5), 7.26 (t, J = 7.3 Hz, 1H, SC_6H_5), 5.87 (d, J = 6.9 Hz, 1H, OH), 5.55 (d, J = 6.4 Hz, 1H, OH), 4.73 (d, J = 9.7 Hz, 1H, H_1), 4.62 (t, J = 5.7 Hz, 1H, $H_{6'}$), 3.69 (ddd, J = 2 0.3, 5.6 and 12.4 Hz, 1H, H_6), 3.51-3.45 (m, 1H, H_5), 3.40 (t, J = 9.5 Hz, 1H, H_3), 3.36-3.31 (m, 1H, H_2), 3.21-3.10 (m, 2H, H_4, OH) ppm. ^{13}C NMR (125 MHz, MeOD): δ 134.9, 133.0, 129.9, 128.5, 89.7, 82.4, 73.1, 72.8, 70.0, 62.6 ppm. HRMS: calcd for $C_{12}H_{15}O_4N_3NaS$ $[M+Na]^+$: 320.0675; found 320.0675 (−0.2805 ppm). M.p:156–159 °C. $[\alpha]_D^{20}$: 52.8 (c 1, CH_3OH).

Phenyl 3-azido-4,6-O-benzylidene-1,3-dideoxy-1-thio-D-glucopyranoside, (18(α,β)). To a solution of 3.7 g of the mixture of the two anomers **17α** and **17β** (12.60 mmol) and 0.09 g of CSA (0.40 mmol) in 150 mL of DMF, 2.9 mL of dimethoxymethyl benzene (18.90 mmol) was added at room temperature. The reaction was allowed to rotate at 35 °C in the rotavapor for 26 h. After the starting product was consumed, the reaction mixture was quenched with saturated $NaHCO_3$ (1 x 40 mL) solution. The aqueous phase was extracted with CH_2Cl_2 (2 x 60 mL) and the combined organic phases were dried over anhydrous Na_2SO_4 and the solvent was evaporated under reduced pressure. The crude obtained was purified by flash column chromatography (hexane: AcOEt 10:1) to obtain 3.4 g of a mixture of the two anomers **18α** and **18β** in a ratio of α:β 0.09:1 (8.80 mmol, 70 % yield) as a white solid.

Phenyl 3-azido-4,6-O-benzylidene-1,3-dideoxy-1-thio-α-D-glucopyranoside, (18α). ^{1}H NMR (500 MHz, $CDCl_3$): δ 7.53-7.50 (m, 2H, SC_6H_5, CHC_6H_5), 7.42-7.36 (m, 3H, CHC_6H_5), 7.36-7.31 (m, 3H, SC_6H_5), 5.59 (s, 1H, H_7), 5.59 (d, J = 5.2 Hz, 1H, H_1), 4.37 (td, J = 4.9 and 9 0.8 Hz, 1H, H_5), 4.31 (dd, J = 5.0 and 10.3 Hz, 1H, $H_{6'}$), 3.92 (ddd, J = 5.4,

7.9 and 13, 4 Hz, 1H, H_2), 3.78 (t, $J = 10.1$ Hz, 1H, H_6), 3.76 (t, $J = 9.8$ Hz, 1H, H_3) 3.56 (t, $J = 9.6$ Hz, 1H, H_4), 2.50 (d, $J = 7.9$ Hz, 1H, OH) ppm. ^{13}C NMR (125 MHz, $CDCl_3$): δ 136.9, 133.1, 132.5, 129.5, 129.3, 128.5, 128.3, 126.2, 101.8, 91.3, 80.0, 71.7, 68.8, 64.6, 64.3 ppm. HRMS: calcd for $C_{19}H_{19}O_4N_3NaS$ $[M+Na]^+$: 408.0988; found 408.0984 (−1.2122 ppm). M.p: 146–148 °C. $[\alpha]_D^{20}$: +303.6 (c 1, $CHCl_3$).

Phenyl 3-azido-4,6-O-benzylidene-1,3-dideoxy-1-thio-β-D-glucopyranoside, (18β). ^{1}H NMR (500 MHz, $CDCl_3$): δ 7.56-7.52 (m, 2H, SC_6H_5), 7.49-7.46 (m, 2H, CHC_6H_5), 7.40-7.33 (m, 3H, SC_6H_5, 3H, CHC_6H_5), 5.56 (s, 1H, H_7), 4.63 (d, $J = 9.7$ Hz, 1H, H_1), 4.40 (dd, $J = 4.8$ and 10.5 Hz, 1H, $H_{6'}$), 3.78 (t, $J = 10.2$ Hz, 1H, H_6), 3.72 (t, $J = 9.4$ Hz, 1H, H_3), 3.59 -3.48 (m, 2H, H_4, H_5), 3.40 (td, $J = 2.5$ and 9.4 Hz, 1H, H_2), 2.61 (d, $J = 2.5$ Hz, 1H, OH) ppm. ^{13}C NMR (125 MHz, CDCl3): δ 136.8, 133.5, 130.9, 129.4, 129.3, 128.9, 128.5, 126.2, 101.7, 89.3, 79.3, 71.9, 71.6, 68.7, 66.1 ppm. HRMS: calcd for $C_{19}H_{19}O_4N_3NaS$ $[M+Na]^+$: 408.0988; found 408.0982 (−1.5529 ppm). M.p: 141–144 °C. $[\alpha]_D^{20}$: 17.5 (c 1, $CHCl_3$).

Phenyl 3-azido-4,6-O-benzylidene-1,3-dideoxy-2-O-(*p*-fluorobenzyl)-1-thio-D-glucopyranoside, (20(α,β)). To a solution of 3.7 g of the mixture of the two anomers **18α** and **18β** (9.60 mmol) in 65 mL of THF, a suspension of 1.2 g of NaH (48.10 mmol) in 10 mL of THF was added. The mixture was allowed to stir for 1 h. After that time, 2.1 g of $INBu_4$ (5.8 mmol) was added and after 30 min stirring, 1.7 mL of *p*-fluorobenzyl chloride (14.40 mmol) was added. The reaction was allowed to stir at room temperature for 24 h. After the starting product was consumed, the reaction mixture was treated with saturated NH_4Cl solution (1 x 25 mL). The aqueous phase was extracted with AcOEt (2 x 50 mL) and the combined organic phases were washed with saturated NaCl solution (1 x 50 mL), dried over anhydrous Na_2SO_4 and the solvent was evaporated under reduced pressure. The crude was purified by flash column chromatography (hexane: AcOEt 20:1) to obtain 4.5 g of a mixture of the two anomers **20α** and **20β** in a ratio of α:β 0.09:1 (9.50 mmol, quant. yield) as a white solid.

Phenyl 3-azido-4,6-O-benzylidene-1,3-dideoxy-2-O-(*p*-fluorobenzyl)-1-thio-α-D-glucopyranoside, (20α). ^{1}H NMR (500 MHz, $CDCl_3$): δ 7.51 (dd, $J = 2.0$ and 7.8 Hz, 2H, CHC_6H_5), 7.46 (dd, $J = 1.8$ and 8.2 Hz, 2H, SC_6H_5), 7.42-7.36 (m, 3H, CHC_6H_5, 2H, FC_6H_4), 7.35-7.29 (m, 3H, SC_6H_5), 7.04 (tt, $J = 2.9$ and 8.7 Hz, 2H, FC_6H_4), 5.60 (d, $J = 5.5$ Hz, 1H, H_1), 5.55 (s, 1H, H_7), 4.76 (d, $J = 11$, 5 Hz, 1H, OCH_2), 4.66 (d, $J = 11.5$ Hz, 1H, OCH_2), 4.40 (td, $J = 4.9$ and 9.9 Hz, 1H, H_5), 4, 20 (dd, $J = 5.0$ and 10.4 Hz, 1H, $H_{6'}$), 3.97 (t, $J = 9.9$ Hz, 1H, H_3), 3.75 (dd, $J = 5.5$ and 9.8 Hz, 1H, H_2), 3.70 (t, $J = 10.3$ Hz, 1H, H_6), 3.47 (t, $J = 9.8$ Hz, 1H, H_4) ppm. ^{13}C NMR (125 MHz, $CDCl_3$): δ 162.8 (d, $J = 247.0$ Hz, FC_6H_4), 136.9, 133.3, 132.8 (d, $J = 3.4$ Hz, FC_6H_4), 132.4, 130.2 (d, $J = 8.2$ Hz, FC_6H_4), 129.3, 129.3, 128.5, 127.9, 126.3, 115.6 (d, $J = 21.3$ Hz, FC_6H_4), 101.9, 87.3, 79.8, 78.3, 72.1, 68.8, 63.7, 62.5 ppm. HRMS: calcd for $C_{26}H_{24}O_4N_3FNaS$ $[M+Na]^+$: 516.1364; found 516.1356 (−1.4209 ppm). M.p: 179–181 °C. $[\alpha]_D^{20}$: +181.9 (c 1, $CHCl_3$).

Phenyl 3-azido-4,6-O-benzylidene-1,3-dideoxy-2-O-(*p*-fluorobenzyl)-1-thio-β-D-glucopyranoside, (20β). ^{1}H NMR (500 MHz, $CDCl_3$): δ 7.55-7.51 (m, 2H, SC_6H_5), 7.49 (dd, $J = 2.1$ and 7.9 Hz, 2H, CHC_6H_5), 7.46-7.41 (m, 2H, FC_6H_4), 7.40-7.31 (m, 3H, SC_6H_5, 3H, CHC_6H_5), 7.06 (tt, $J = 2.8$ and 8.7 Hz, 2H, FC_6H_4), 5.57 (s, 1H, H_7), 4.90 (d, $J = 10.1$ Hz, 1H, OCH_2), 4.79 (d, $J = 10.1$ Hz, 1H, OCH_2), 4.75 (d, $J = 9.7$ Hz, 1H, H_1), 4.38 (dd, $J = 4.7$ and 10.7 Hz, 1H, $H_{6'}$), 3.81-3.74 (m, 2H, H_2, H_5), 3.55-3.46 (m, 2H, H_3, H_6), 3.35 (t, $J = 9.3$ Hz, 1H, H_4) ppm. ^{13}C NMR (125 MHz, $CDCl_3$): δ 162.8 (d, $J = 246.4$ Hz, FC_6H_4), 136.8, 133.3 (d, $J = 2.9$ Hz, FC_6H_4), 132.9, 132.4, 130.5 (d, $J = 8.2$ Hz, FC_6H_4), 129.3, 128.5, 128.3, 126.2, 115.5 (d, $J = 21.7$ Hz, FC_6H_4), 101.6, 88.7, 79.7, 79.3, 75.1, 71.2, 68.8, 67.1 ppm. HRMS: calcd for $C_{26}H_{24}O_4N_3FNaS$ $[M+Na]^+$: 516.1364; found 516.1358 (−1.1560 ppm). M.p: 127–130 °C. $[\alpha]_D^{20}$: 28.2 (c 1, $CHCl_3$).

(*R*)-{1-[3,5-bis(trifluoromethyl)phenyl] ethyl}3-azido-4,6-O-benzylidene-3-deoxy-2-O-(*p*-fluorobenzyl)-D-glucopyranoside, (8(α,β)). To a solution of 1.0 g of the mixture of both anomers **20α** and **20β** (2.10 mmol), 0.5 g of (*R*)-1-[3,5-bis(trifluoromethyl)phenyl] ethanol (2.10 mmol) and 0.5 g of NIS (2.10 mmol) in 20 mL of CH_2Cl_2, in the presence of 4 Å molecular sieve previously activated in the microwave and in vacuo, in the absence of light and under an argon atmosphere, 0.04 mL of TMSOTf (0.20 mmol) was added dropwise, at 0 °C and left stirring at room temperature. Once the starting product was consumed, after a reaction time of 3 h, the reaction mixture was quenched with 2.0 mL of Et_3N (14.7 mmol) and filtered. The organic phase was washed with saturated $Na_2S_2O_3$ solution (1 x 30 mL), saturated $NaHCO_3$ solution (1 x 30 mL) and saturated NaCl solution (1 x 30 mL), dried over anhydrous Na_2SO_4 and the solvent was evaporated under reduced pressure. The crude obtained was purified by flash column chromatography (hexane: AcOEt 40:1) to obtain 0.6 g of a mixture of the two anomers **8α** and **8β** in a ratio of α:β 5:1 (0.90 mmol, 43 % yield) as white solids.

(*R*)-{1-[3,5-bis(trifluoromethyl)phenyl] ethyl} 3-azido-4,6-O-benzylidene-3-deoxy-2-O-(*p*-fluorobenzyl)-α-D-glucopyranoside, (8α). Yield: 36%. ^{1}H NMR (500 MHz, $CDCl_3$): δ 7.90 (bs, 2H, $CF_3C_6H_3$), 7.86 (bs, 1H, $CF_3C_6H_3$), 7.52 (dd, $J = 1.8$ and 7.8 Hz, 2H, CHC_6H_5), 7.42-7.36 (m, 3H, CHC_6H_5), 7.18-7.12 (m, 2H, FC_6H_4), 6.95 (tt, $J = 2.8$ and 8.7 Hz, 2H, FC_6H_4), 5.57 (s, 1H, H_7), 4.91 (c, $J = 6.6$ Hz, 1H, $OCHCH_3$), 4.58 (d, $J = 3.4$ Hz, 1H, H_1), 4.57 (d, $J = 11.9$ Hz, 1H, OCH_2), 4.51 (d, $J = 11.9$ Hz, 1H, OCH_2), 4.34 (dd, $J = 4$, 9 and 10.3 Hz, 1H, $H_{6'}$), 4.15 (t, $J = 9.9$ Hz, 1H, H_3), 3.98 (td, $J = 4.8$ and 10.0 Hz, 1H, H_5), 3.73 (t, $J = 10.4$ Hz, 1H, H_6), 3.45 (t, $J = 9.7$ Hz, 1H, H_4), 3.30 (dd, $J = 3.6$ and 9.9 Hz, 1H, H_2), 1.58 (d, $J = 6.6$ Hz, 3H, $OCHCH_3$) ppm. ^{13}C NMR (125 MHz, $CDCl_3$): δ 162.7 (d, $J = 246.9$ Hz, FC_6H_4), 145.3 ($CF_3C_6H_3$), 136.8, 132.8 (d, $J = 3.4$ Hz, FC_6H_4), 132.2 (q, $J = 33.4$ Hz, $CF_3C_6H_3$), 130.0, 129.9 (d, $J = 8.2$ Hz, FC_6H_4), 129.3, 128.5, 127,0 (bs, $CF_3C_6H_3$), 126.1, 123.4 (q, $J = 272.7$ Hz, $CF_3C_6H_3$), 122.1 (sept, $J = 3.6$ Hz, $CF_3C_6H_3$), 115.5 (d, $J = 21.4$ Hz, FC_6H_4), 101.7, 95.1, 80.3, 73.3, 72.7, 69.1, 63.4, 62.0, 24.4 ppm. HRMS: calcd for $C_{30}H_{26}O_5N_3F_7Na$ $[M+Na]^+$: 664.1653; found 664.1649 (−0.5659 ppm). M.p: 98–100 °C. $[\alpha]_D^{20}$: +17.3 (c 1, $CHCl_3$).

(*R*)-{1-[3,5-bis-(trifluoromethyl)phenyl] ethyl} 3-azido-4,6-O-benzylidene-3-deoxy-2-O-(*p*-fluorobenzyl)-β-D-glucopyranoside, (8β). Yield: 7%. ^{1}H NMR (500 MHz, $CDCl_3$): δ 7.81 (bs, 3H, $CF_3C_6H_3$), 7.47 (dd, $J = 2.3$ and 7.8 Hz, 2H, CHC_6H_5), 7.41-7, 34 (m, 3H, CHC_6H_5, 2H, FC_6H_4), 7.07 (tt, $J = 2.8$ and 8.7 Hz, 2H, FC_6H_4), 5.51 (s, 1H, H_7), 4.98 (q, $J = 6.5$ Hz, 1H, $OCHCH_3$), 4.91 (d, $J = 10.8$ Hz, 1H, OCH_2), 4.81 (d, $J = 10.8$ Hz, 1H, OCH_2), 4.69 (d, $J = 7.6$ Hz, 1H, H_1), 4.15 (dd, $J = 4.9$ and 10.6 Hz, 1H, $H_{6'}$), 3.70 (t, $J = 9$ 0.7 Hz, 1H, H_3), 3.63 (t, $J = 10.3$ Hz, 1H, H_6), 3.46 (t, $J = 9.6$ Hz, 1H, H_4), 3.40-3 0.33 (m, 2H, H_2, H_5), 1.58 (d, $J = 6.5$ Hz, 3H, $OCHCH_3$) ppm. ^{13}C NMR (125 MHz, $CDCl_3$): δ 162.7 (d, $J = 246.5$ Hz, FC_6H_4), 145.8 ($CF_3C_6H_3$), 136.8, 133.4 (d, $J = 3.3$ Hz, FC_6H_4), 131.7 (q, $J = 33.2$ Hz, $CF_3C_6H_3$), 130.2 (d, $J = 8.3$ Hz, FC_6H_4), 129.3, 128.5, 126.5 (bs, $CF_3C_6H_3$), 126.1, 123.5 (q, $J = 272.6$ Hz, $CF_3C_6H_3$), 121.6 (sept, $J = 3.8$ Hz, $CF_3C_6H_3$), 115.6 (d, $J = 21.4$ Hz, FC_6H_4), 102.8, 101.6, 80.5, 79.1, 76.8, 74.7, 68.5, 67.2, 65.0, 22.6 ppm. HRMS: calcd for $C_{30}H_{26}O_5N_3F_7Na$ $[M+Na]^+$: 664.1653; found 664.1648 (−0.7934 ppm). M.p: 111–114 °C. $[\alpha]_D^{20}$: 16.2 (c 1, $CHCl_3$).

(*R*)-{1-[3,5-bis-(trifluoromethyl)phenyl] ethyl}3-azido-3-deoxy-2-O-(*p*-fluorobenzyl)-α-D-glucopyranoside, (9α). To a solution of 0.1 g of **8α** (0.20 mmol) in 6 mL of methanol, a catalytic amount of CSA was added at room temperature. Once the starting product is consumed, after a reaction time of 3 h and 30 min, the reaction mixture was quenched with 4.6 μL of Et_3N (0.03 mmol). The solvent was evaporated under reduced pressure and evaporated twice with toluene. The crude was purified by flash column chromatography (hexane:AcOEt 1:1) to obtain 0.055 g of **9α** (0.10 mmol, 61 % yield) as a white solid. ^{1}H NMR (500 MHz, $CDCl_3$): δ 7.88 (bs, 2H, $CF_3C_6H_3$), 7.85 (bs, 1H, $CF_3C_6H_3$), 7.17-7.12 (m, 2H, FC_6H_4), 6.94 (tt, $J = 2.9$ and 8.7 Hz, 2H, FC_6H_4), 4.90 (q, $J = 6.6$ Hz, 1H, $OCHCH_3$), 4.60 (d, $J = 3.4$ Hz, 1H, H_1), 4.51 (d, $J = 11.9$ Hz, 1H, OCH_2), 4.42 (d, $J = 11.9$ Hz, 1H, OCH_2), 3.96 (t, $J = 9.9$ Hz, 1H, H_3), 3.90-3.82 (m, 2H, H5, $H_{6'}$), 3.78 (dt, $J = 3.8$ and 9.7 Hz, 1H, H_4), 3.45 (t, $J = 9.6$ Hz, 1H, H_6), 3.28 (dd, $J = 3.4$ and 10.2 Hz, 1H, H_2), 1.55 (d, $J = 6$, 6Hz, 3H, $OCHCH_3$) ppm. ^{13}C NMR (125 MHz, $CDCl_3$): δ 162.7 (d, $J = 246.5$ Hz, FC_6H_4), 145.4 ($CF_3C_6H_3$), 132.8 (d, $J = 3.4$ Hz,

FC_6H_4), 132.2 (q, J = 33.4 Hz, $CF_3C_6H_3$), 129.9 (d, J = 8.2 Hz, FC_6H_4), 126.9 (bs, $CF_3C_6H_3$), 123.4 (q, J = 272 0.9 Hz, $CF_3C_6H_3$), 122.2 (sept, J = 3.7 Hz, $CF_3C_6H_3$), 115.5 (d, J = 21.5 Hz, FC_6H_4), 94.0, 77.3, 73.1, 72.3, 71.4, 69.4, 65.4, 62.2, 24.4 ppm. HRMS: calcd for $C_{23}H_{22}O_5N_3F_7Na$ $[M+Na]^+$: 576.1340; found 576.1333 (−1.1661 ppm). M.p: 160–162 °C. $[\alpha]_D^{20}$: +28.9 (c 1, $CHCl_3$).

(*R*)-{1-[3,5-bis(trifluoromethyl)phenyl] ethyl}3-azido-3-deoxy-2-O-(*p*-fluorobenzyl)-β-D-glucopyranoside, (9β). To a solution of 0.06 g of **8β** (0.09 mmol) in 3.5 mL of methanol, a catalytic amount of CSA was added at room temperature. Once the starting product was consumed, after a reaction time of 3 h and 30 min, the reaction mixture was quenched with 2.5 μL of Et_3N (0.02 mmol), the solvent was evaporated under reduced pressure and evaporated twice with toluene. The crude was purified by flash column chromatography (hexane:AcOEt 2:1) to obtain 0.03 g of **9β** (0.05 mmol, 60 % yield) as a white solid. ^{1}H NMR (500 MHz, $CDCl_3$): δ 7.82 (bs, 2H, $CF_3C_6H_3$), 7.81 (bs, 1H, $CF_3C_6H_3$), 7.40-7.36 (m, 2H, FC_6H_4), 7.06 (tt, J = 2.9 and 8.7 Hz, 2H, FC_6H_4), 4.97-4.91 (m, 1H, $OCHCH_3$, 1H, OCH_2), 4.78 (d, J = 10.8 Hz, 1H, OCH_2), 4.64 (d, J = 7.6 Hz, 1H, H_1), 3.69-3.61 (m, 2H, H_5, $H_{6'}$), 3.46 (t, J = 9.5 Hz, 1H, H_6), 3.42 (t, J = 9.4 Hz, 1H, H_3), 3.35 (t, J = 8.6 Hz, 1H, H_2), 3.27 (dt, J = 4.1 and 8.9 Hz, 1H, H_4), 1.57 (d, J = 6.5 Hz, 3H, $OCHCH_3$) ppm. ^{13}C NMR (125 MHz, $CDCl_3$): δ 162.8 (d, J = 246.3 Hz, FC_6H_4), 146.3 ($CF_3C_6H_3$), 133.3 (d, J = 3.2 Hz, FC_6H_4), 131.7 (q, J = 33.3 Hz, $CF_3C_6H_3$), 130.3 (d, J = 8.1 Hz, FC_6H_4), 126.4 (bs, $CF_3C_6H_3$), 123.4 (q, J = 272.7 Hz, $CF_3C_6H_3$), 121.6 (sept, J = 3.9 Hz, $CF_3C_6H_3$), 115.7 (d, J = 21.5 Hz, FC_6H_4), 102.8, 79.9, 77.1, 75.7, 74.3, 69.3, 68.7, 62.3, 22.9 ppm. HRMS: calcd for $C_{23}H_{22}O_5N_3F_7Na$ $[M+Na]^+$: 576.1340; found 576.1334 (−0.9485 ppm). M.p: 116–118 °C. $[\alpha]_D^{20}$: 23.4 (c 1, $CHCl_3$).

(*R*)-{1-[3,5-bis-(trifluoromethyl)phenyl] ethyl}3-amino-4,6-O-benzylidene-3-deoxy-2-O-(*p*-fluorobenzyl)-α-D-glucopyranoside, (10α). To a solution of 0.08 g of **8α** (0.10 mmol) in 3 mL of THF, under an argon atmosphere and at 0 °C, was added, dropwise 0.05 mL of $LiAlH_4$ solution (0.10 mmol). Once the starting product was consumed, after a reaction time of 1 h, the reaction was hydrolyzed with 0.04 mL of saturated Na_2SO_4 solution, and the suspension obtained was filtered through a pad of Celite and washed with THF (30 mL). The filtrate was evaporated under reduced pressure and the crude was purified by flash column chromatography (TBME) to obtain 0.05 g of **10α** (0.08 mmol, 67 % yield) as a yellow solid. ^{1}H NMR (500 MHz, $CDCl_3$): δ 7.90 (bs, 2H, $CF_3C_6H_3$), 7.85 (bs, 1H, $CF_3C_6H_3$), 7.50 (dd, J = 2.2 and 7.8 Hz, 2H, CHC_6H_5), 7.40-7.36 (m, 3H, CHC_6H_5), 7.17-7.13 (m, 2H, FC_6H_4), 6.95 (t, J = 8.6 Hz, 2H, FC_6H_4), 5.53 (s, 1H, CHC_6H_5), 4.94 (q, J = 6.6 Hz, 1H, $OCHCH_3$), 4.67 (d, J = 3.4 Hz, 1H, H_1), 4.50 (d, J = 11.8 Hz, 1H, $OCH_2C_6H_4$), 4.33 (dd, J = 4.9 and 10.3 Hz, 1H, $H_{6'}$), 4.30 (d, J = 11.8 Hz, 1H, $OCH_2C_6H_4$), 3.95 (td, J = 4.9 and 10.0 Hz, 1H, H_5), 3.73 (t, J = 10.3 Hz, 1H, H_6), 3.59 (t, J = 9.7 Hz, 1H, H_3), 3.37 (t, J = 9.6 Hz, 1H, H_4), 3.33 (dd, J = 3.5 and 9.8 Hz, 1H, H_2), 1.58 (d, J = 6.6 Hz, 3H, $OCHCH_3$) ppm. ^{13}C NMR (125 MHz, $CDCl_3$): δ 162.7 (d, J = 246.7 Hz, FC_6H_4), 145.7 ($CF_3C_6H_3$), 137.3, 133.1 (d, J = 2.9 Hz, FC_6H_4), 132.2 (q, J = 33.3 Hz, $CF_3C_6H_3$), 129.9 (d, J = 8.2 Hz, FC_6H_4), 129.3, 128.5, 126.9 (bs, $CF_3C_6H_3$), 126.3, 123.4 (q, J = 272.9 Hz, $CF_3C_6H_3$), 122.1 (sep, J = 3.6 Hz, $CF_3C_6H_3$), 115.6 (d, J = 21.8 Hz, FC_6H_4), 101.9, 94.4, 82.0, 79.9, 73.1, 72.1, 69.2, 63.2, 51.4, 24.4 ppm. HRMS: calcd for $C_{30}H_{29}O_5NF_7$ $[M+H]^+$: 616.1928; found 616.1922 (−1.0343 ppm). M.p: 87–90 °C. $[\alpha]_D^{20}$: +75.1 (c 1, $CHCl_3$).

(*R*)-{1-[3,5-bis-(trifluoromethyl)phenyl] ethyl}3-amino-3-deoxy-2-O-(*p*-fluorobenzyl)-α-D-glucopyranoside, (11α). To a solution of 49.6 mg of **9α** (0.05 mmol) in 3 mL of THF, under an argon atmosphere and at 0 °C, was added, dropwise 0.04 mL of $LiAlH_4$ solution (0.09 mmol). Once the starting product was consumed, the reaction was hydrolyzed with 0.05 mL of saturated Na_2SO_4 solution, and the suspension obtained was filtered through a pad of Celite and washed with THF (30 mL). The filtrate was evaporated under reduced pressure and the crude was purified by flash column chromatography (EtOAc:MeOH 6:1) to obtain 27.5 mg of **11α** (0.05 mmol, 58 % yield) as a white solid. ^{1}H NMR (500 MHz, $CDCl_3$): δ 7.87-7.84 (m, 3H, $CF_3C_6H_3$), 7.14-7.11 (m, 2H, FC_6H_4), 6.94-6.91 (m, 2H, FC_6H_4), 4.88 (q, J = 6.8 Hz, 1H, $OCHCH_3$), 4.69 (d, J = 3.1 Hz, 1H, H_1), 4.41-4.34 (m, 2H, OCH_2 and $H_{6'}$), 4.24 (d, J = 11.2 Hz, 1H, OCH_2), 3.92-3.90 (m, 2H, OH and H_5), 3.78 (bs, H, OH), 3.71-3.66 (m, 2H, H_3 and H_6), 3.44-3.35 (m, 2H, H_2 and H_4), 1.97 (s, 2H, NH_2), 1.53 (d, J = 6, 6 Hz, 3H, $OCHCH_3$) ppm. ^{13}C NMR (125 MHz, $CDCl_3$): δ 162.8 (d, J = 246.9 Hz), 145.8, 133.4 (d, J = 3.0 Hz), 132.2 (q, JCF = 33.4 Hz), 129.9 (d, J = 8.2 Hz), 126.9 (q, J = 3.8 Hz), 123.4 (q, J = 271.8 Hz), 122.0 (sept, JCF = 3.8 Hz), 115.7 (d, J = 21.3 Hz), 95.1, 75.9, 73.4, 72.2, 70.9, 69.9, 69.1, 63.5, 24.5 ppm. HRMS: calcd for $C_{23}H_{24}O_5NF_7Na$ $[M+Na]^+$: 550.4258; found 550.4256 (−1.0341 ppm).

4.2. Molecular modelling

In order to validate the docking method used with AutoDock Vina, we redocking three co-crystalized ligands exiting with NKR1 protein: CP-99,994 (PDB ID: 6HLL), Aprepitant (PBB ID: 6HLO) and Netupitant (PDB IDs: 6HLP) and then compare the obtained cartesian coordinates of the docked ligand atoms with those of the native ones, using root mean square deviation values (RMSD). All the predicted docking poses presented RMSD values lower than 1.5 Å (0.893 Å for CP-99,994, 1.242 Å for Aprepitant and 1.075 Å for Netupitant), when compared to the experimentally co-crystallized binding pose [7]. These results indicate that the used molecular docking protocol using AutoDock Vina is satisfactory for inferring the correct binding modes and the interactions of such ligands with NKR1.

Molecular structure of the ligands were optimized in the ground state at the DFT level with the B3LYP [25–27] and the 6-31G (d,p) basis set [28,29] implemented in the Gaussian 09 Rev.D.O1 package programs [30]. Molecular docking calculations were performed by AutoDock Vina [31] and AutodockTools Software [32]. The structure of NKR1 were retrieved from the Protein Data Bank (PDB ID: 6HLO) and all water molecules and co-crystallized ligand were removed from crystallographic structures to prepare the docking receptor. The best docking poses and interactions involved in the binding mode was visualized with Discovery Studio Visualizer (Accelrys Software Inc.) [33]. LogP (octanol/water partition coefficient) values of the ligands were calculated from the Molinspiration server (http://www.molinspiration.com/) by providing SMILES code of the fragments of the ligands as input.

4.3. Biological studies

4.3.1. Survival analysis

Kaplan-Meier survival curves from publicly available dataset (Gene Expression Omnibus; http://www.ncbi.nlm.nih.gov/geo; accession: GSE16476) were performed using the R2 microarray analysis and visualization platform (http://r2.amc.nl). The Kaplan scanning tool in the R2 platform was used to check for mRNA expression in a dataset of 88 neuroblastoma tumors. Expression data were scanned to find the optimal cut-off between high and low gene expression and the log-rank test performed to calculate p-values. P-values were corrected for multiple testing (one-way ANOVA). Differences between groups expressing high and low TACR1 mRNA levels were considered significant when p-value was below 0.01.

4.3.2. Real time q-PCR analysis

Real time quantitative PCR (q-PCR) was performed by using ABI PRISM 7500 Fast Sequence Detection System instrument and software (Applied Biosystem, Foster City, CA). Relative quantification of target cDNA in each sample was performed from 10 ng of cDNA, kindly supplied for PhD. Isabel Martinez, from different neuroblastoma cell lines (IMR32, Kelly, Lan1, Lan5, NGP and SH-SY5Y), HeLa cell line and the Retinal Pigmented Epithelial (RPE) Cells as non-tumoral cell line. We used SYBR-Green One-Step real time PCR Master Mix with specific primers for fl-NK1R and tr-NK1R [5]. For fl-NK1R: Forward, 5′-AACCCCATCATCTACTGCTGC-3′ and reverse, 5′-

ATTTCCAGCCCCTCATAGTCG-3' (NM_001058.3) and for tr-NK1R forward, 5′-GGGCCACAAGACCATCTACA-3′ and reverse, 5′- AAGTTAGCTGCAGTCCCCAC-3' (NM_015727.2); β-actin was used as housekeeping gene: Forward 5′-GCCTCGCCTTTGCCGATC-3′ and reverse 5′-CCCACGATGGAGGGGAAG-3'. Primers were supplied by Sigma. The amplification of the housekeeper was done in parallel with the gene to be analyzed. Thus, the results were normalized using the β-actin expression. Threshold cycle (Ct) values were calculated using the software supplied by Applied Biosystems. Data was expressed as arbitrary units [mean ± SEM (n = 3)]. Significant differences compared with RPE1 cells evaluated by one-way ANOVA test, followed by a Bonferroni post-hoc test. The significance was set at 95% of confidence.

4.3.3. Cell culture

Human neuroblastoma cell lines Kelly and SH-SY5Y were purchased from the German Collection of Microorganisms and Cell Cultures (Leibniz Institute DSMZ, Braunschweig, Germany). Human retina epithelial cells RPE-1 cells were purchased from the American Type Culture Collection (ATCC, Manassas, US). Cells were maintained at 37 °C in a humidified 5% CO2 atmosphere in DMEM (SHSY5Y), DMEMF12 (RPE-1) or RPMI (Kelly) all of them supplemented with 10% of heat inactivated fetal bovine serum, 100 U/mL penicillin and 100 U/mL streptomycin. Cells were subcultured every 3–4 days.

4.3.4. Cell viability assay

Cell viability was determined by using the 3-(4,5-dimethyl-2-thiazolyl)-2,5-diphenyl-2H-tetrazolium bromide (MTT) colorimetric assay (Sigma-Aldrich). Cells were plated in 96-well microplates at a 3 x 105 cells mL-1 density. After 24 h cells were treated for 72h with increasing concentrations of 1(α,β) to **11α** compounds, ranged between 0 and 400 μM for 1(α,β), **3α**, 3**β, 5 (α,β)**, **6β**, between 0 and 50 μM for **2α**, **2β**, **7α**, **9β**, **10α** and between 0 and 100 μM for **4α**, **4β**, **6α**, **7β, 11α** and Aprepitant. Three replicates for each point and plate were performed to obtain dose-response curves. Cell viability was determined by colorimetric evaluation using a Synergy HT Biotech spectrophotometer at 555 and 690 nm in at least three independent experiments. Viability for each concentration was calculated as the ratio of the mean optical density of treated cells relative to untreated cells and expressed as a percentage. Calculation of half maximal inhibitory concentration (IC50) was conducted by fitting a regression curve to the viability data. Results were expressed as the means ± standard error of the mean (SEM).

4.3.5. Flow cytometry assays

For the evaluation of the apoptotic effect of the carbohydrate-based Aprepitant analogs, cells were seeded in 12-well plates overnight and treated with 20 or 40 μM of **2α**, **2β**, **7β**, **7α** for 48h. Apoptosis was determined by Annexin-V/PI method using the PE Annexin V Apoptosis Detection Kit I (BD Biosciences) following manufacturer's instructions. The effect of these compounds on proliferation was evaluated using propidium iodide (PI/RNAse solution, Immunostep) and cell cycle analysis by flow cytometry. Briefly, cells were seeded in 12-well plates and treated with 20 or 40 μM of **2α**, **2β**, **7β**, **7α**. After 48h, cells were harvested, fixed and stained with PI following manufacturer's instructions. All flow cytometry analyses were performed using an Accuri C6 Flow Cytometer (BD Biosciences).

All experiments were performed three times independently. Data are presented as the mean ± SEM. Statistical significance between groups was performed using a two-sided Student's *t*-test. Differences were considered to be statistically significant when P values were less than 0.05.

Supporting information

^{1}H NMR, and ^{13}C NMR spectra of all new products, docking and biological data are included in Supporting Information.

CRediT authorship contribution statement

Victoria Valdivia: Formal analysis, Investigation, Methodology, Supervision. **Rocío Recio:** Data curation, Formal analysis, Methodology, Supervision, Writing – original draft, Writing – review & editing. **Patricia Lerena:** Formal analysis, Investigation, Methodology. **Esther Pozo:** Formal analysis, Investigation, Methodology. **Rosario Serrano:** Investigation, Methodology. **Raúl Calero:** Investigation, Methodology. **Cristina Pintado:** Formal analysis, Investigation. **Manuel Pernia Leal:** Methodology, Supervision. **Nazaret Moreno-Rodríguez:** Investigation. **Juan Ángel Organero:** Investigation, Methodology. **Noureddine Khiar:** Conceptualization, Methodology. **Inmaculada Fernández:** Conceptualization, Data curation, Funding acquisition, Methodology, Project administration, Resources, Supervision, Writing – review & editing.

Declaration of competing interest

The authors declare that they have no known competing financial interests or personal relationships that could have appeared to influence the work reported in this paper.

Data availability

No data was used for the research described in the article.

Acknowledgment

This work was supported by the Ministerio de Ciencia, Innovación y Universidades (grant number PID2019-104767RB-I00) cofinanced by the European Regional Development Fund (ERDF) from FEDER. We gratefully thank the Centre of Research Technology and Innovation of the University of Seville (CITIUS) for NMR facilities.

Appendix A. Supplementary data

Supplementary data to this article can be found online at https://doi.org/10.1016/j.ejmech.2023.116021.

Abbreviations

NK1R	neurokinin 1 receptor
fl-NK1R	full-length neurokinin 1 receptor
tr-NK1R	truncated neurokinin 1 receptor
GlucoK1RAnt	D-glucose-based NK1R antagonists
SP	substance P
NB	neuroblastoma
DAG	diaceton-D-glucose
DMF	dimethylformamide
THF	tetrahydrofuran
HMRS	high-resolution mass spectra
NMR	nuclear magnetic resonance spectroscopy

References

[1] K.R. Bosse, J.M. Maris, Advances in the translational genomics of neuroblastoma: from improving risk stratification and revealing novel biology to identifying actionable genomic alterations, Cancer 122 (1) (2016) 20–33.
[2] J.M. Maris, M.D. Hogarty, R. Bagatell, S.L. Cohn, J.M. Maris, M.D. Hogarty, R. Bagatell, S.L. Cohn, Lancet 369 (2007) 2106–2120.
[3] M. Berger, D. Von Schweinitz, Therapeutic innovations for targeting childhood neuroblastoma: implications of the neurokinin-1 receptor System, Anticancer Res. 37 (11) (2017) 5911–5918.
[4] S. Garcia-Recio, P. Gascón, Biological and pharmacological aspects of the NK1-receptor, BioMed Res. Int. (2015) 1–14.
[5] A. Pohl, R. Kappler, J. Mühling, D. Von Schweinitz, M. Berger, Expression of truncated neurokinin-1 receptor in childhood neuroblastoma is independent of tumor biology and stage, Anticancer Res. 37 (11) (2017) 6079–6085.

[6] A.G. Henssen, A. Odersky, A. Szymansky, M. Seiler, K. Althoff, A. Beckers, F. Speleman, S. Schäfers, K. De Preter, K. Astrahanseff, J. Struck, A. Schramm, A. Eggert, A. Bergmann, J.H. Schulte, Targeting tachykinin receptors in neuroblastoma, Oncotarget 8 (1) (2017) 430–443.
[7] R. Recio, P. Lerena, E. Pozo, J.M. Calderón-Montaño, E. Burgos-Morón, M. López-Lázaro, V. Valdivia, M. Pernia Leal, B. Mouillac, J.Á. Organero, N. Khiar, I. Fernández, Carbohydrate-based NK1R antagonists with broad-spectrum anticancer activity, J. Med. Chem. 64 (14) (2021) 10350–10370.
[8] J.J. Molenaar, J. Koster, D.A. Zwijnenburg, P. Van Sluis, L.J. Valentijn, I. Van Der Ploeg, M. Hamdi, J. Van Nes, B.A. Westerman, J. Van Arkel, M.E. Ebus, F. Haneveld, A. Lakeman, L. Schild, P. Molenaar, P. Stroeken, M.M. Van Noesel, I. Øra, E.E. Santo, H.N. Caron, E.M. Westerhout, R. Versteeg, Sequencing of neuroblastoma identifies chromothripsis and defects in neuritogenesis genes, Nature 483 (7391) (2012) 589–593.
[9] S.-C. Huang, V.L. Korlipara, Neurokinin-1 receptor antagonists: a comprehensive patent survey, Expert Opin. Ther. Pat. 20 (2010) 1019–1045.
[10] M. Muñoz, J. Martinez-Armesto, R. Coveñas, Expert Opin. Ther. Pat. 22 (2012) 735–746.
[11] G.A. Giardina, S. Gagliardi, M. Martinelli, Antagonists at the neurokinin receptors-recent patent literature, Idrugs 6 (2003) 758–772.
[12] G.R. Efremov, O.A. Chugunov, V.T. Pyrkov, P.J. Priestle, S.A. Arseniev, E. Jacoby, Molecular lipophilicity in protein modeling and drug design, Curr. Med. Chem. 14 (4) (2007) 393–415.
[13] F. Desantis, M. Miotto, L. Di Rienzo, E. Milanetti, G. Ruocco, Spatial organization of hydrophobic and charged residues affects protein thermal stability and binding affinity, Sci. Rep. 12 (1) (2022), 12087.
[14] P. Zhou, J. Zou, F. Tian, Z. Shang, Fluorine bonding — how does it work in Protein−Ligand interactions? J. Chem. Inf. Model. 49 (2009) 2344–2355.
[15] L.M. Salonen, M. Ellermann, F. Diederich, Aromatic rings in chemical and biological recognition: energetics and structures, Angew. Chem. Int. 50 (2011) 4808–4842.
[16] J.E. DeLorbe, J.H. Clements, M.G. Teresk, A.P. Benfield, H.R. Plake, L. E. Millspaugh, F.M. Stephen, Thermodynamic and structural effects of conformational constraints in Protein−Ligand interactions. Entropic paradoxy associated with ligand preorganization, J. Am. Chem. Soc. 131 (2009) 16758–16770.
[17] E. Barratt, A. Bronowska, J. Vondrášek, J. Černý, R. Bingham, S. Phillips, S. W. Homans, Thermodynamic penalty arising from burial of a ligand polar group within a hydrophobic pocket of a protein receptor, J. Mol. Biol. 362 (2006) 994–1003.
[18] S.M. Christensen, H.F. Hansen, T. Koch, Molar-scale synthesis of 1,2:5,6-Di-0-Isopropylidene-α-D- allofuranose: DMSO oxidation of 1,2:5,6-Di-0-Isopropylidene-α-D- glucofuranose and subsequent sodium borohydride reduction, Org. Process Res. Dev. 8 (5) (2004) 777–780.
[19] V.K. Sharma, M. Kumar, C.E. Olsen, A.K. Prasad, Chemoenzymatic convergent synthesis of 2'-o,4'-c-Methyleneribonucleosides, J. Org. Chem. 79 (13) (2014) 6336–6341.
[20] Z.G. Gao, H.T. Duong, T. Sonina, S.K. Kim, P. Van Rompaey, S. Van Calenbergh, L. Mamedova, H.O. Kim, M.J. Kim, A.Y. Kim, B.T. Liang, L.S. Jeong, K.A. Jacobson, Orthogonal activation of the reengineered A3 adenosine receptor (neoceptor) using tailored nucleoside agonists, J. Med. Chem. 49 (9) (2006) 2689–2702.
[21] A.S. Figueredo, L.O.B. Zamoner, M. Rejzek, R.A. Field, I. Carvalho, Cluster glycosides and heteroglycoclusters presented in alternative arrangements, Tetrahedron Lett. 59 (50) (2018) 4405–4409.
[22] A.P. Wang, C. Liu, S. Yang, Z. Zhao, P. Lei, An efficient method to synthesize novel 5-O-(6′-Modified)-Mycaminose 14-membered ketolides, Tetrahedron 72 (2) (2016) 285–297.
[23] N. Khiar, I. Fernández, R. Recio, M. López-Lázaro, J.M. Calderón-Montaño, Antagonistas de los Receptores NK1 Derivados de Hidratos de Carbono, Método de Obtención y Uso Médico, 2016. WO2016189179A1.
[24] M. Muñoz, R. Coveñas, The neurokinin-1 receptor antagonist aprepitant: an intelligent bullet against cancer? Cancers 12 (2020) 2682.
[25] A.D. Becke, Density-functional thermochemistry. III. The role of exact exchange, J. Chem. Phys. 98 (1993) 5648–5652.
[26] A.D. Becke, Density-functional thermochemistry. I. The effect of the exchange-only gradient correction, J. Chem. Phys. 96 (1992) 2155–2160.
[27] C. Lee, W. Yang, R.G. Parr, Development of the colle-salvetti correlation-energy formula into a functional of the electron density, Phys. Rev. B 37 (1988) 785–789.
[28] W.J. Hehre, R. Ditchfield, J.A. Pople, Self—consistent molecular orbital methods. XII. Further extensions of Gaussian—type basis sets for use in molecular orbital studies of organic molecules, J. Chem. Phys. 56 (1972) 2257–2261.
[29] M.M. Francl, W.J. Pietro, W.J. Hehre, J.S. Binkley, M.S. Gordon, D.J. DeFrees, J. A. Pople, Self-consistent molecular orbital methods. Xxiii. A polarization-type basis set for second-row elements, J. Chem. Phys. 77 (1982) 3654–3665.
[30] M.J. Frisch, G.W. Trucks, H.B. Schlegel, G.E. Scuseria, M.A. Robb, J.R. Cheeseman, G. Scalmani, V. Barone, G.A. Petersson, H. Nakatsuji, X. Li, M. Caricato, A. Marenich, J. Bloino, B.G. Janesko, R. Gomperts, B. Mennuci, H.P. Hratchian, J. V. Ortiz, A.F. Izmaylov, J.L. Sonnenberg, D. Williams-Young, F. Ding, F. Lipparini, F. Egidi, J. Goings, B. Peng, A. Petrone, T. Henderson, D. Ranasinghe, V. G. Zakrzewski, J. Gao, N. Rega, G. Zheng, W. Liang, M. Hada, M. Ehara, K. Toyota, R. Fukuda, J. Hasegawa, M. Ishida, T. Nakajima, Y. Honda, O. Kitao, H. Nakai, T. Vreven, K. Throssell, J.A. Montgomery Jr., J.E. Peralta, F. Ogliaro, M. Bearpark, J.J. Heyd, E. Brothers, K.N. Kudin, V.N. Staroverov, T. Keith, R. Kobayashi, J. Normand, K. Raghavachari, A. Rendell, J.C. Burant, S.S. Iyengar, J. Tomasi, M. Cossi, J.M. Milam, M. Klene, C. Adamo, R. Cammi, J.W. Ochterski, R.L. Martin, K. Morokuma, O. Farkas, J.B. Foresman, D.J. Fox, Gaussian 09, Revision A.02, Gaussian Inc., Wallingford, Connecticut, 2016. EE.UU.
[31] O. Trott, A.J. Olson, AutoDock Vina: improving the speed and accuracy of docking with a new scoring function, efficient optimization, and multithreading, J. Comput. Chem. 31 (2010) 455–461.
[32] G.M. Morris, R. Huey, W. Lindstrom, M.F. Sanner, R.K. Belew, D.S. Goodsell, A. J. Olson, AutoDock4 and AutoDockTools4: automated docking with selective receptor flexibility, J. Comput. Chem. 30 (2009) 2785–2791.
[33] Discovery Studio Visualizer, Version 4.0.; Software for Viewing, Sharing, and Analyzing Protein and Modeling Data, BIOVIA, San Diego, EE.UU, 2012.